Science Requirements Document
SRD Version 2.0
March 31, 2010
for

ELECTRIC FIELD CONTROL OF FLAMES
E-FIELD Flames Experiment

Principal Investigator:

Derek Dunn-Rankin
University of California
Irvine, California

Co-Investigators:

Felix Weinberg; Imperial College, London
Zeng-Guang Yuan, National Center for Space Exploration Research (NCSER)

Project Scientist:

Dennis Stocker, NASA GRC

EXECUTIVE SUMMARY

This project utilizes electric fields in microgravity combustion science to establish a fundamental understanding of chemi-ionization and ion-driven convection in flames. It also uses this understanding to demonstrate electrical manipulation of sooting behavior and stability limits in the absence of buoyancy. This work is based on prior foundation studies that included simulating zero-g combustion of small gas jet diffusion flames in an earth-gravity laboratory, and the electric field control of flame electrodynamics. The current SRD proposes to use the extended-duration microgravity environment to further develop an understanding of electric fields in combustion processes and their potential applications.

The research centers on the fact that electrical forces, acting on charge carriers created through chemi-ionization, can provide for measurement and manipulation of flames in microgravity environments. For example, using the drag exercised on flame ions, electric fields have demonstrated powerful influences on flame shape, sooting behavior, burning velocity, extinction, and stability. The source of these influences resides in ion wind effects. In microgravity, where there are no density-driven buoyant effects to contend with, ion winds represent an important (and perhaps the only) body force that can be applied to manipulate combustion systems. This project includes both academic study of electric field effects and aspects for practical utilization of electrical control of combustion processes.

Our prior laboratory experiments have shown that electrical properties of flames can be used to produce enhanced combustion performance by: (a) manipulating flame ions in order to change flame chemistry – this is generally considered a minor influence because flame ion concentration is typically small, but it may be critical at near-limit conditions; (b) creating a neutral wind (ion driven convection) locally at the flame front – this process can provide a local actuator for flame convection control; (c) using electric fields to affect soot formation and transport – ions and soot are closely linked because there are shared chemical pathways and because soot particles are charged by the flame ions; and (d) using electrical properties to characterize flames – e.g., there is a relationship between flame temperature, the carbon content of a fuel, and the ion current it can produce at saturation.

In 1-g, the above-mentioned processes are confounded by complex buoyancy interactions that cannot be unraveled. Hence, to evaluate them in detail, we propose the following experimental objectives for an extended microgravity environment: (A) determine the relationship between electric field voltage and chemi-ion current as functions of total fuel flow rate and the amount of inert (nitrogen) in the fuel; (B) compare the time response of the flame's chemiluminescence and ion current to rapid changes in electric fields; (C) determine sooting behavior in relation to the electric field influences; and (D) manipulate the limit behavior of lifted flames using electric fields.

The experimental approach includes a simple gas jet diffusion flame and a co-flow burner. The basic variations in the tests are in the burner type, the fuel type (nominally non-sooting and sooting), and in the level of inert dilution of the fuel to vary the flame strength. The co-flow or environment gas will have a nominal molar composition of 21% O_2 and 79% N_2. The experimental concept is to ground the burner to the test chamber

and to install an electrically active planar mesh electrode downstream of the burner mouth. The potential of the mesh electrode can be either positive or negative, with a steady voltage or with a time varying potential (including a rapid step change) to examine the flame's steady state response and time response. The data to be recorded include the applied voltage, the ion current, the flame broadband luminosity, the CH* luminosity, flame images of OH* and visible light showing the flame shape as a function of electric potential and flame shape changes during transients in the electric field. In addition, a desired measurement of temperature in and near the flame will monitor the thermal field as a function of the electric field conditions.

The data from these measurements will allow a chemical and physical understanding of flame ion production and information showing the potential to use these ions to electrically control the flame both via modification of the local chemistry near extinction limits and through changes in the local convection using the ion driven wind. For example, a lifted diffusion flame near its blowoff condition is sensitive to mixing at the flame anchor point. Therefore, electric fields acting on near-limit flames can exert a large influence because they can affect the local mixing behavior. The role of electric fields on soot formation will be dramatic under conditions where the ion driven wind has a large influence on flow residence time (or on ion residence time, if chemical effects are found important) in sooting flames.

Generally, the convective flows driven by electric fields acting on flame ions and those driven by buoyancy have been found to be of the same order of magnitude in earth gravity. In addition, raising the temperature often increases the ion production rate and the response to an electric field, but increasing temperature also increases the buoyancy effect, making it difficult, on earth, to separate ion wind effects from those due to buoyancy. In the zero-g environment, it will be possible to eliminate the buoyancy confusion and develop sufficient understanding to predict the response of flames to electric fields under all conditions. Extended run times are crucial for all of the studies because the timescales of flame property changes (which includes chemi-ionization) are dominated by convection (length scale/velocity) and past studies have shown that soot studies require high quality zero gravity timescales longer than is available in aircraft and drop towers. In addition, exploring instabilities and extinction behavior in near-limit flames requires experiments lasting tens of seconds.

Overall, the goal of this zero-gravity study is to understand chemi-ionization behavior and the resulting ion driven winds sufficiently well so that electrical properties of flames can be used to characterize (by monitoring ion current) and control them (via direct chemical or local convective influences). Electric field effects on flames have been documented for decades (even centuries), but flames in 1-g all include buoyancy influences that affect ion generation behavior. For flames near transitions and limits, buoyant influences always confound any understanding of the role of ion driven winds in using electric fields to characterize and manipulate flames. The proposed study removes this confounding influence and allows definitive measurement and analysis of the electric field effects on jet diffusion and co-flow flames.

TABLE OF CONTENTS

Nomenclature

Constants

g	gravitational acceleration, $9.81 m/s^2$
e	fundamental charge, $1.602\times10^{-19} C$
ε_o	permittivity of free space, $8.85\times10^{-12} C^2/N/m^2$

Scalar Symbols

Φ	electric potential field
ε	permittivity of the ambient gas, $C^2/N/m^2$
q	space charge density, C/m^3
$\vec{j}$	local current density, $C/(m^2)$
K	ion mobility, $m^2/V\ s$
D	ion diffusion coefficient, m^2/s
$\vec{E}$	electric field, N/C
$\vec{V}$	gas velocity, m/s
$q\nabla\Phi$	Coulomb force, N
$\vec{F}$	external body force per unit volume, N/m^3
$\vec{\tau}$	stress tensor
ρ	density, kg/m^3
P	static pressure
S	entropy, $J/s/K$
W	Power, Watts
I	ion current, Amps
V	electric potential, *Volts*
R_{sense}	sense resistor, Ω

Abbreviations

ACME	advanced combustion through microgravity experiments
CLD	co-flow laminar diffusion
E-FIELD	electric-field effects on laminar diffusion
FID	flame ionization detector
TFP	thin filament pyrometry
VCC	voltage-current curve
HV	high voltage
ppb	parts per billion
cc	cubic centimeter
sccm	cubic centimeters per minute at STP

1 INTRODUCTION

The first subsection provides the fundamentals that link chemi-ionization in flames with convective flows created when electric fields act on the ions generated. Later subsections describe the variety of 1-g laboratory experiments exemplifying the scientific data we have found valuable in linking flames to their electrical properties. For the purposes of this SRD, the details of this introductory section are less important than the examples of our preliminary results which inform our proposed selection of objectives and science data end products. To focus on the proposed flight experiment, it is possible to skip directly to Section 1.4 and then refer to background information as needed.

1.1 Background and Overview of Ion Driven Winds in Flames

In addition to being a major liberator of chemical energy, hydrocarbon flames naturally produce charged intermediate species (ions and electrons) during the chemical-to-thermal energy conversion. Generally speaking, chemi-ions and their associated species in hydrocarbon flames do not participate substantially in the major heat release reaction pathways. Hence, the chemical kinetics of ion species in hydrocarbon flames has not been studied as extensively as for those species or reaction mechanisms associated with ignition/extinction phenomena and pollutant formation. Nevertheless, many of the chemical kinetic pathways are fairly well articulated. Figure 1.1 shows the chemi-ion pathways from Starik and Titova [1] and Pederson and Brown [2]. The major ions are formed through reactions which involve CH molecules. The CH molecules are formed either from acetylene and other C_2 molecules, or via the oxidation of CH_3. Green and Sugden [3] proposed that CH is produced in a methane/air stoichiometric mixture primarily via the oxidation of CH_3 through $CH_3+O \rightarrow CH+H_2O$. Peeters et al. [4] have used this reaction successfully in their computations, and Jones et al. [5] examined modifying the rate constant of this reaction to result in a better correlation with experimental observations. Pederson and Brown [2] used a 13-step reaction scheme for the determination of the ion profiles. Their results indicate that for a stoichiometric mixture, H_3O^+ is the most important ion; its maximum concentration is more than two orders of magnitude higher than that of $C_2H_3O^+$ and $C_3H_3^+$, and three orders of magnitude higher than that of HCO^+. The latter ion is, however, an important component for the production of H_3O^+. Prager, et al. examined ion chemistry more recently and found H_3O^+ to be dominant in lean flames [6]. They also identified several areas of uncertainty, primarily the anion (negative ion) chemistry. Despite these uncertainties, there is general agreement in the

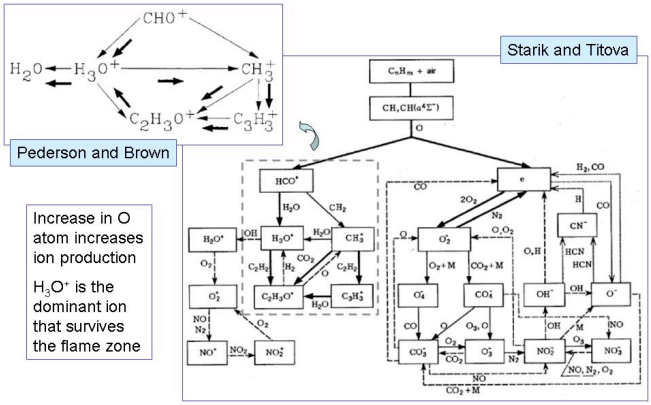

Figure 1. 1. Principal pathways of hydrocarbon flame ion chemistry

literature that the weak plasma nature of flames is relatively unimportant for the heat release reactions. For example, the most populous cations (positive ions) are present in peak concentrations on the order of 10^{10}/cc, or with mole fractions in the range of 10 ppb.

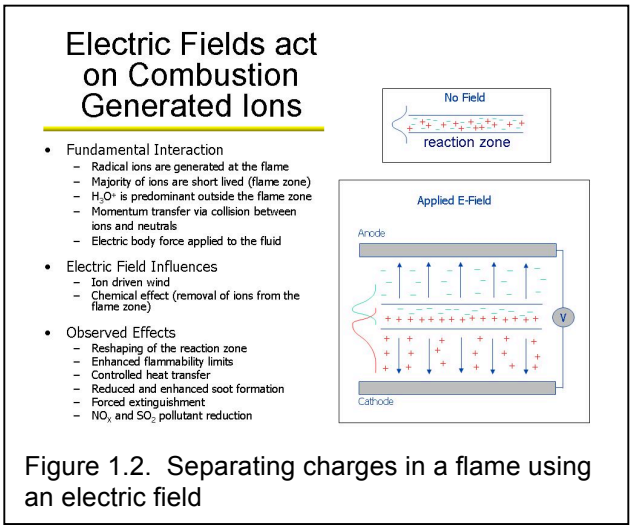

Figure 1.2. Separating charges in a flame using an electric field

The concentration of electrons (which make up the majority of the negative charge carriers) is even lower than the concentration of positive ions because electron mobility is very high so that relatively few electrons are needed to balance the charge flux carried by the more massive and more populous positive charge carriers. Nevertheless, the free charges in the flame make the reaction zone a very good conductor (similar to that of a conductive metal). More importantly, if an electric field is applied across the flame, the charges can be separated into unipolar regions, as shown in Figure 1.2. In the case where the anode (higher potential electrode) is close to the flame, the electrons can then easily exit the gas phase system, leaving the positive ions to collide with neutral molecules as they migrate through the unipolar space between the flame and the cathode (lower potential electrode). During this migration process, the ions impart momentum to the neutral gas equivalent to the acceleration they have achieved in the electric field between mean-free-path collisions. The collisions are so frequent, that the ions quickly establish a drift velocity governed by their mobility. The collisions thereby link the ionization processes to the neutral gas flow. This phenomenon is referred to as a Chattock wind, an ion-wind, or more accurately an ion-driven wind, and is described in some detail by Lawton and Weinberg [7].

In all of the applications involving electrical generation of convection, a unidirectional gas flow is induced by using a large electric field to act on the charges of a unipolar ion cloud in the region between the ion source and a second, usually earthed, electrode, or set of electrodes. In these cases, the body force on a unit volume of the gas is equal to that on the charges it contains, provided that they have a constant mobility and do not accelerate. In atmospheric pressure systems, the latter condition on acceleration is met easily, but in regions of high temperature gradients or changes in chemical composition, the constant mobility condition is not. Fortunately, these regions are often of limited spatial extent and so the effects of variable mobility are usually ignored. As described, for example in references [8,9] isothermal ion driven flow (with constant mobility) is described generally by the coupled equations of fluid continuity and momentum along with an electrical model, including, Poisson's equation governing the electric field,

$$\nabla^2 \Phi = -\frac{q}{\varepsilon}$$

where Φ is the scalar electric potential, q is the space charge density, and ε is the permittivity of the ambient gas. The charge drifts through the ambient gas as described by

$$\vec{j} = q(K\vec{E} + \vec{V}) - D\nabla q,$$

where $\vec{j}$ is the current density, K is the ion mobility, D is the ion diffusion coefficient, E is the electric field strength, and $\vec{V}$ is the gas velocity responsible for charge convection. Charge conservation is governed by,

$$\nabla \cdot \vec{j}.$$

After assuming that ion transport is dominated by electrical forces so that ion diffusion and ion convection can be neglected (both good assumptions in high electric fields), the charge conservation equation reduces to [9],

$$\nabla q \cdot \nabla \Phi = \frac{q^2}{\varepsilon}.$$

To fully simulate the system, an ion source model is needed as a boundary condition for the charge conservation equation. Accurately modeling the details of the flame ion source chemistry is difficult, and providing data to improve such models is one important goal of this project. Fortunately, in some applications the source region is so small that a constant ion source of sufficient intensity to account for the overall current flow in the system can provide an appropriate charge concentration boundary.

We assume a steady, laminar air flow with constant properties that satisfies the continuity equation,

$$\nabla \cdot \vec{V} = 0$$

and the momentum equation,

$$\nabla \cdot (\rho \vec{V}\vec{V}) = -\nabla P + \nabla \cdot \bar{\bar{\tau}} + \vec{F},$$

where P is the static pressure, $\bar{\bar{\tau}}$ is the stress tensor, and $\vec{F}$ is the external body force per unit volume that can include buoyancy, $\rho\vec{g}$ and the Coulomb force, $q\nabla\Phi$. It is this last term that couples the neutral gas flow to the ion motion.

In order to gain some physical insight into the ion driven wind and its relationship to system parameters, we can describe a theoretical one-dimensional configuration, where a planar ion source at high potential is separated from a planar ground electrode. Under these conditions, the body force applied to the neutral gas is [8]

$$F_{\pm} = Ee(q_{\pm})$$

and the local current density, j,

$$j = K_{\pm} q_{\pm} Ee$$

so that

$$F_{\pm} = j / K_{\pm},$$

where e and q represent fundamental charge and number density of charges, respectively, and the sign in the subscript denotes the polarity. This unipolar condition applies so long as the field at the target electrode(s) does not reach magnitudes large enough to cause secondary ionization and electrical breakdown of the neutral gas there. Beyond breakdown, F decreases because the secondary ions counterflow and neutralize those driving the process. The space charge causes E to grow in the inter-electrode region and the consequent eventual electrical breakdown generally determines the maximum effects that can be achieved. Extending the unidimensional concept suggests that the distribution of body force and consequent pressure gradients results in gas flow which can be tailored by appropriate design of the electrode geometry. Under ideal circumstances, forces can be achieved that are hundreds of times those of buoyancy [10], but in typical combustion situations, the ion driven wind will be on the order of a few m/s and the force achieved will be a few times that of buoyancy. Although this may not seem substantial, ion driven winds have been used to extinguish flames [11].

The above equations show that an electric field applied to the flame can create a direct body force, or force per unit volume, on the system just as buoyancy does in a gravitational field. Because buoyancy can be a dominant characteristic of terrestrial combustion processes, it may seem less than obvious why physics regards gravity as a "weak force." However, if we consider a small magnet picking up a metal object with the entire earth pulling in the opposite direction, it becomes obvious how much stronger the electromagnetic forces are. It is hardly surprising, therefore, that electrical forces acting on charge carriers can effectively substitute for gravitational influences or, more generally, provide for vigorous combustion control in its absence (i.e., in microgravity). It is the opportunity for exploiting the electric force in flames that motivates this research activity. Already, electric fields have demonstrated powerful influences on combustion processes that include flame shape [12,13], sooting behavior [14-16], burning velocity [17,18], extinction [11,19], and stability [20,21]. The foundation of many of these results, as discussed in Lawton and Weinberg [7], reside in ion wind effects. In microgravity, where there are no density driven buoyant effects to contend with, ion winds represent an important (and perhaps the only) body force that can be applied to manipulate combustion systems. Hence, the zero gravity environment provides a unique opportunity to probe and exploit the electrical aspects of flames [22].

1.2 Opportunities in Microgravity for Understanding Electric Field Effects on Flames

There are at least four ways that detailed measurements of electrical properties of flames in microgravity can be used to improve our understanding of flame electrochemistry and to potentially improve combustion performance:

(1) Extracting flame ions in order to change flame chemistry – we have already described that ion radicals are not considered a large contributor to combustion heat release. However, in the situations of weak flames, as can be represented by diluted diffusion flames in zero gravity and terrestrial flames near extinction limits, their role is likely to be more important. In addition, in near-limit flames, ion manipulation may be used to extend stability behavior.

(2) Creating a neutral wind (ion driven convection) locally at the flame front; this is one of the rare and important action-at-a-distance effects on flames that can be used as a localized actuator. A one dimensional estimate of the equation for the forces available shows that the typical values for a flame can produce ion winds with flow velocity on the order of 1 m/s and forces on the order of one or two times the buoyant force. Although this sounds like a fairly modest wind, it has been shown to be capable of substantial effects, including flame extinction [11,19]. The effect of the wind has been demonstrated with a candle flame in parabolic flight based microgravity [12] and in a spherical cage drop tower [13], but there has been no systematic study of the ion wind effect in the absence of the confounding effects of the approximately equal influence of buoyancy. The actuation of the flame can be used to control flame performance despite external fluctuations.

(3) Using electric fields to affect soot formation and transport – ions and soot are closely linked because there are shared chemical pathways [23] and because soot particles are charged by the flame ion attachment or electron ejection. It is possible, therefore, to modify soot formation and to use charges attached to soot to affect soot transport. By adjusting the soot trajectory through the reaction zone it is possible to affect the oxidation of soot to prevent its eventual release or to modify the residence time of soot in different zones of the flame. It is also possible to use the neutral ion wind to change the mixing behavior of the flame and reduce soot in this way.

(4) Using the electrical properties to characterize the flame – there is a quantifiable relationship between the carbon content of a fuel and the ion current it can produce at saturation [24]. This relationship is already exploited in a typical flame ionization detector (FID) analyzer for hydrocarbon emission where the carbon is burned in a hydrogen flame to create an ion current in proportion to the carbon influx. In direct flame interrogation, however, there are several confounding variables that can affect the ion current, including flame temperature (which generally affects the O atom concentration) and the reaction zone volume. Flame temperature can in turn be affected by levels of premixing, diffusion rates, fuel composition, and radiative loss. It is possible, therefore, to determine flame character from the ionization curve response. There are also many opportunities identified for ion sensors as part of a combustion

control scheme, where input variables can be tuned to optimal performance as measured by ion current. HCCI engines, for example, would benefit from an in-cylinder diagnostic to determine the combustion quality [6,25].

Examples of the kinds of methods and phenomena described above are provided in the next subsection.

1.3 Results from Earth Gravity Experiments

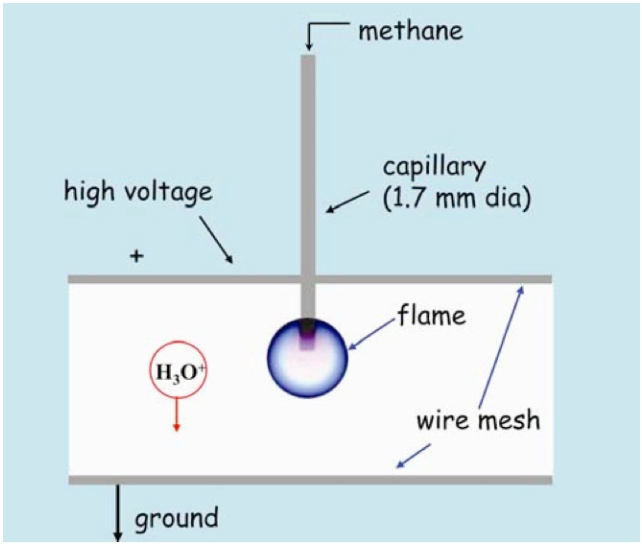

Figure 1.3. Experimental apparatus for capillary flame under electric field control.

A series of 1-g experiments were performed in order to demonstrate some of the phenomena described above. In the following sections we outline some examples of tailored ion driven gas flows. Among applications based on flame ions, we describe electric field-controlled flame convection in actual microgravity environments [11,26], as well as the creation of microbuoyancy by the application of electric fields to flames in the laboratory [27,28]. The final set of 1-g studies use electric fields to actively control flame luminosity and ion current [29,30]. The basic experimental configuration for nearly all of these studies is shown in Figure 1.3. It consists of a small diffusion flame burning at the end of a metal capillary (1.7 mm o.d.) between two planar mesh electrodes. The metal capillary is kept at the same potential as the mesh electrode with which it has contact. One important aspect of this geometry is that when it is charged positively, the capillary acts an electrode that draws away electrons, letting the positive ions produce a uni-polar wind. Recent tests with a coflow burner use a similar configuration, the only differences being the burner geometry and a non-inverted orientation.

Electric field-induced flame convection in microgravity [11,26]

While currently, combustion in spacecraft is considered primarily in the context of fire safety, it is possible in the more distant future that combustion may play a role in onboard manufacturing and waste processing. Perhaps more importantly, however, studying electric field-induced convection in microgravity clarifies the fundamentals of this process by eliminating the confounding buoyancy forces. Under earth gravity, diffusion flames rely on natural or forced convection to replenish reactants and direct the hot products. In microgravity, diffusion flames tend to become spherical and, as the result of blanketing by

their own products, burn very slowly under diffusion control and become unsuitable for transferring focused heat to any object.

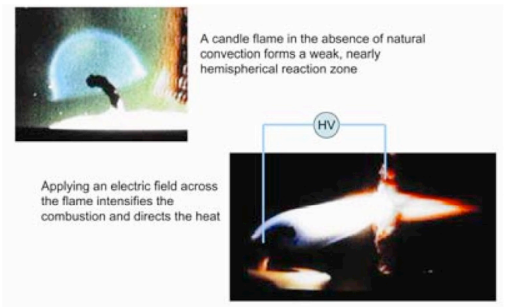

Figure 1.4. Microgravity candle flame with and without electric field forcing.

In the course of work carried out in KC135 parabolic flights, a compact, lightweight electro-gas-dynamic duct using the drag exercised on flame ions was employed to control the gas flow and focus the heat transfer. Figure 1.4 shows images of these early experiments. The positive electrode contacted the flame, allowing for virtually dragless removal of electrons. The metal grid cathode at the end of the duct was used to "focus" the hot product stream. Even with just candle flames, heat fluxes of approximately 300W/cm^2 could be attained. Control of heat transfer from flames, by electric fields, had previously been demonstrated in the laboratory [31]. In space environments, this method can provide intense heating of small areas, making economic use of the oxygen available, offering perhaps the only simple means of allowing combustion of condensed fuels to be used for practical purposes, including for example, stabilizing and reducing waste materials onboard spacecraft.

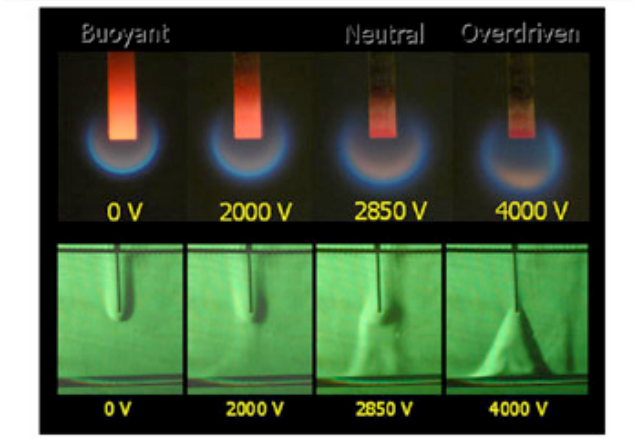

Figure 1.5. Images of 1.8 mm o.d. capillary flames under electric field influence; bottom images are schlieren; black horizontal lines are electrode mesh.

Similar efforts for heat flux control in a droplet stream flame were unsuccessful because the geometry did not include an electrode in contact with the flame [32]. In this case, the ion wind produces a mixing effect that shortens the flame by mixing satellite droplets in unstable streams but has no effect on stable droplet stream flames. This result indicates the importance of having one electrode close to the reaction zone when creating an ion wind.

Creating microbuoyancy by the application of electric fields to flames [27,28,33]

Microgravity is involved in combustion research for eliminating natural convection. To achieve such a condition in the laboratory, natural convection has been counter-balanced against the body force created by flame ions drifting in electric fields. As shown schematically in Figure 1.3, small diffusion flames on metal capillary anodes (higher potential electrodes) were exposed to fields drawing positive ions to permeable cathodes (lower

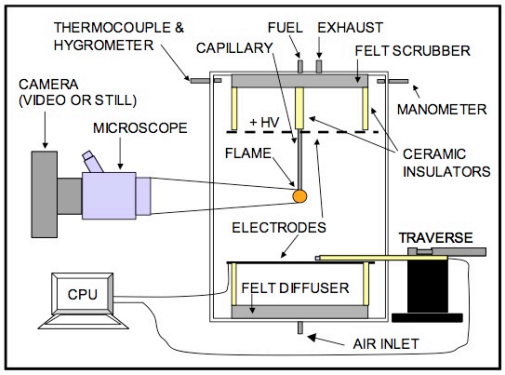

Figure 1.6. Refined apparatus showing the ion probe

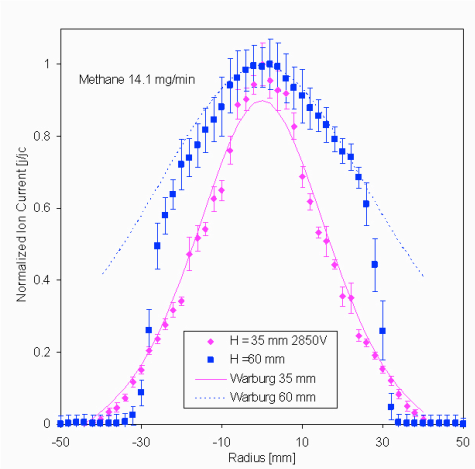

Figure 1.7. Ion flux at the ground electrode

potential electrodes) placed below them. Such bench-top simulations facilitate the use of many optical and laser diagnostic methods that can probe the structure of small diffusion flames.

In preliminary experiments [27], a temporary (of the order of seconds) point of balance was achieved which is, however, inherently unstable and suitable only for instantaneous "snapshot" recording. As shown in Figure 1.5, video recording of shadowgraphy by argon ion laser illumination was employed to monitor the flow of hot gas. The most direct indications of when the point of balance has been reached are that the flame luminosity becomes symmetrical around the burner mouth and that the shadow rapidly vanishes. The diffusion-controlled flame structure causes optical records depending on refractive index gradients to weaken and eventually to disappear.

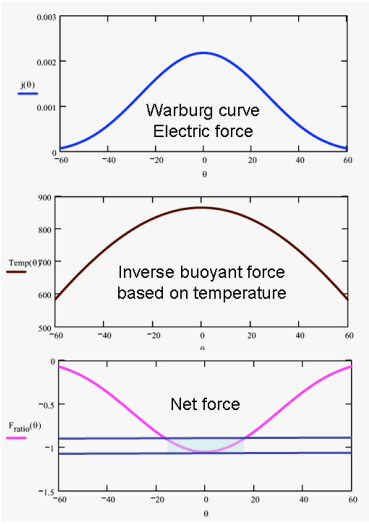

Figure 1.8. Theoretical ion wind force balance based on a symmetric thermal profile and Warburg ion distribution.

In later experiments, the addition of an upper mesh electrode helped stabilize the approximate balance condition for longer periods, and created a localized steady-state balance condition. This permitted iterative measurements over extended time periods, which has been achieved by confining the balance to only part of the flame. The temperature field of a small diffusion flame under electric field control was probed with holographic interferometry [28], N_2 coherent anti-Stokes Raman spectroscopy (CARS) [28,33], and oxygen laser induced fluorescence [33]. Over a portion of the flame, the temperature distribution of such capillary flames closely approximate to the purely diffusive thermal profiles that would be expected under microgravity conditions. The schlieren images of Figure 1.5 show the difficulty in balancing the body force and ion wind force everywhere. The contrast area shows the hot gas which, at balance, should be spherical. However, even at the nominal balance condition (2850 V) as deter-

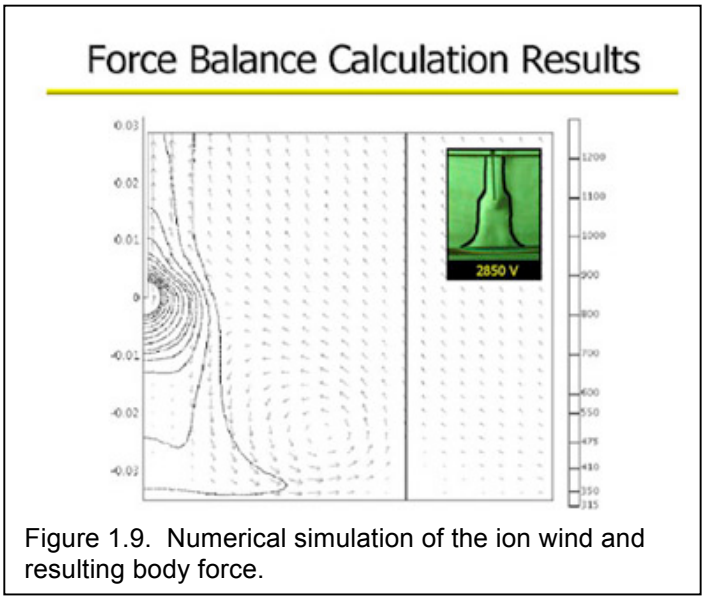

Figure 1.9. Numerical simulation of the ion wind and resulting body force.

mined by the axial temperature profile and the spherical flame boundary, there remains a distinct column of hot gas. To understand the challenge to balance, we measured the ion flux distribution at the ground plane for the small flame. The apparatus for this measurement, which is shown in Figure 1.6, is essentially the same as is shown in Figure 1.3 except that we added the capability of an ion probe flush with the ground mesh to measure the spatial distribution of the ion current. Remarkably, as shown in Figure 1.7, the ion flux follows very closely the Warburg distribution (a profile that describes the space charge distribution for ions generated in a point-to-plane corona discharge). This result indicates that the ion distribution in the unipolar region of the flame system is largely driven by charge repulsion. Knowing the local current density, and then assuming a spherical thermal profile, it is possible to compare approximately the local force balance between buoyancy and the ion driven body force. The comparison is shown in Figure 1.8. From this figure it is clear that balance can only be achieved over a portion of the flame.

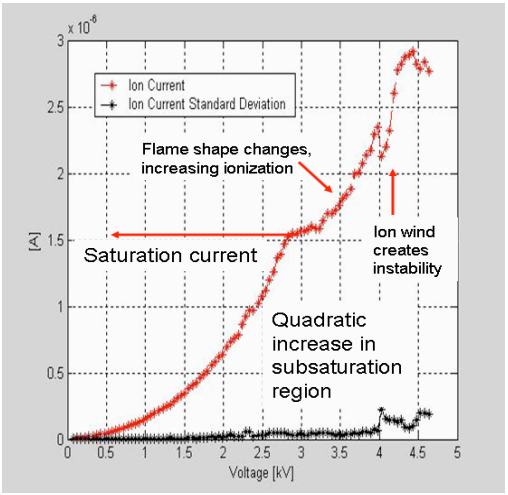

Figure 1.10. Typical voltage-current characteristic curve for diffusion flame.

Our first attempt to simulate the coupled physics of the problem involved computing the flow field associated with the balance condition shown above. The simulation solves the equations described in the background section but also includes variable temperature and the associated buoyant force. The modeling details are too complex to repeat here but they are provided in the references [9,34]. Briefly, the simulation uses the commercial software FEMLAB (now COMSOL Multiphysics) to solve the relevant multi-physics equation with boundary conditions consistent with planar electrodes and the flame acting as a spherical ion source. Figure 1.9 shows the flow field generated by the combination of buoyancy and the ion wind under the capillary flame conditions approximating the balance condition. There are several substantial approximations in this model. One is that there is no chemistry in the simulation. The flame is simply a constant temperature boundary (at the measured flame temperature) and a constant ion

source (at the measured total ion flux). In addition, the flame remains spherical despite any convection from the local ion-driven wind. This model neglects, therefore, the couplings between temperature and the ion source strength and the effects of flows on the flame shape that also change the temperature and the ion source. As mentioned earlier, for these small flames that are space charge dominated, the shape of the flame is unlikely to have a large effect on the shape of the ion flux distribution but it can have a very dramatic effect on the total ion concentration and hence the electric body force.

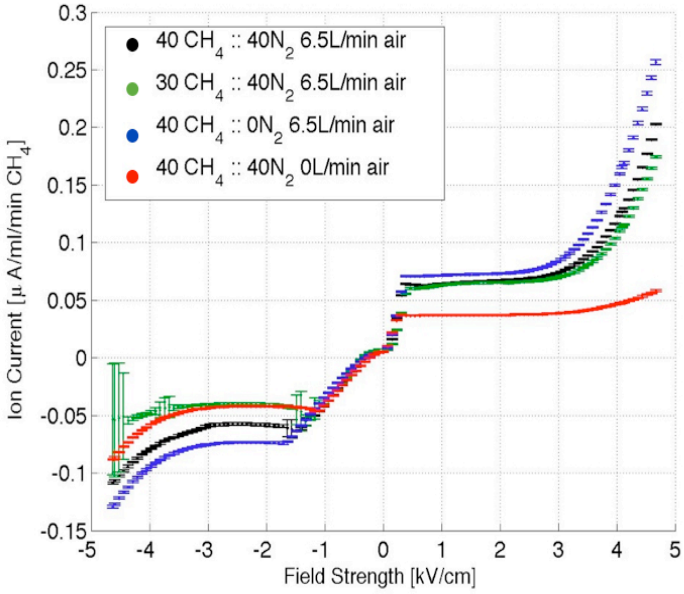

Figure 1.11 Voltage-current characteristic curves for the 1-g coflow burner under negative and positive mesh electric fields.

Effects of different fuels and orientation to gravity on the V-I curve

One of the important findings of the earth gravity studies was how the ion current measurements (i.e., the voltage-current or VI curve) responded to changes in fuel flow rate, flame shape, and the fuel type. A typical VI curve for our small diffusion flames is shown in Figure 1.10. There are three main regions of the curve. At low voltage the current follows a quadratic increase with voltage up to saturation. At saturation, the current is drawn from the flame as rapidly as it can produce ions so there is no further increase in current at this plateau. In this figure, the plateau is quite short, but other conditions give a more pronounced saturation region. We postulated, and demonstrated numerically [35], that the current rises at higher voltages because the ion-driven wind has changed the character of the nominally diffusion flame to one with air entrainment and premixing, which affects the temperature, flame surface area, and the chemistry. The VI curve shows more fluctuation at higher voltages indicating flame instability.

Laboratory electric field experiments were also undertaken using a coflow burner to explore the possibility of using the same burner being considered for other experiments in the ACME program. Electric field experiments on a coflowing flame have shown some similar behaviors to those of the jet diffusion flame, but there are also important differences. Figure 1.11 shows the coflow flame ion current response under different flow conditions. With a negatively charged mesh, low mobility cations drift toward the mesh, entraining additional air in the flame. This additional convective flow causes saturation to occur at different field strengths. The effects of entrainment are not as dramatic when the

mesh is positively charged, and the flame saturates at the same applied electric field strength regardless of flow conditions.

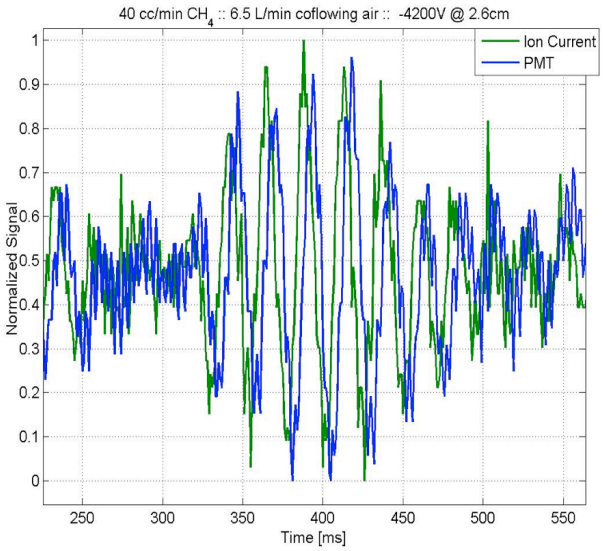

Figure 1.12. Transient ion current and PMT signals under the influence of a static field

For all coflow burner tests, the flames are slightly lifted above the burner surface. Regardless of polarity, electric fields stabilize and draw a lifted flame to the burner. Positive field stability results from the movement of low mobility ions and the corresponding ion wind. Changing polarity, a negative field initially destabilizes the flame, until saturation, where the dominant force changes and the flame is drawn toward the burner. During this transition, the flame oscillates before finally stabilizing. The frequency of this oscillation varies with both jet and coflowing air velocity.

Depending on the condition, the applied field can induce transient ion current oscillations or oscillations in the visible flame. Figure 1.12 shows the transient ion current and PMT response of a flame that does not appear to oscillate because the timescales are too fast to create a noticeable visual effect on the flame. The flame body oscillations, mentioned above, likely result from a competition between the upward directed ion-wind and oxygen-entrained premixing, drawing the flame to the burner. As the flame propagates toward the burner, the amount of entrained oxygen decreases and the dominating force shifts to the ion wind.

Recent experiments are aimed at understanding gravity's influence on the effects of ion-driven winds have been performed using the NASA 2.2 Second Drop Tower. The burner used for the Drop Tower is slightly different in geometry from our 1-g studies at UCI. A detailed discussion of the differences can be found in reference [38]. The behavior of voltage-current characteristic (VCC) curves in the converging nozzle co-flow diffusion flame system (without a honeycomb annulus at the jet exit) exhibited features of both the co-flow burner flames (with a honeycomb) and downward facing jet diffusion flames in still air (without a honeycomb). As a result of the relatively high mean fuel jet and co-flow air velocities (> 25 cm/s), flame shape and ion current were similar in 1g and μg. This makes clear the gravity effect on global responses of the flame such as the ion current were minimal and unrepresentative at these conditions. These results offered interesting insights. As the magnitude of the negative field was increased, the flame became slender, soot formation was suppressed, and the flame base gradually lifted from the fuel

tube as a result of ion-induced flow entrainment toward the flame tip. At applied voltages near the saturation transitions, the flame oscillated significantly as the flame base par-

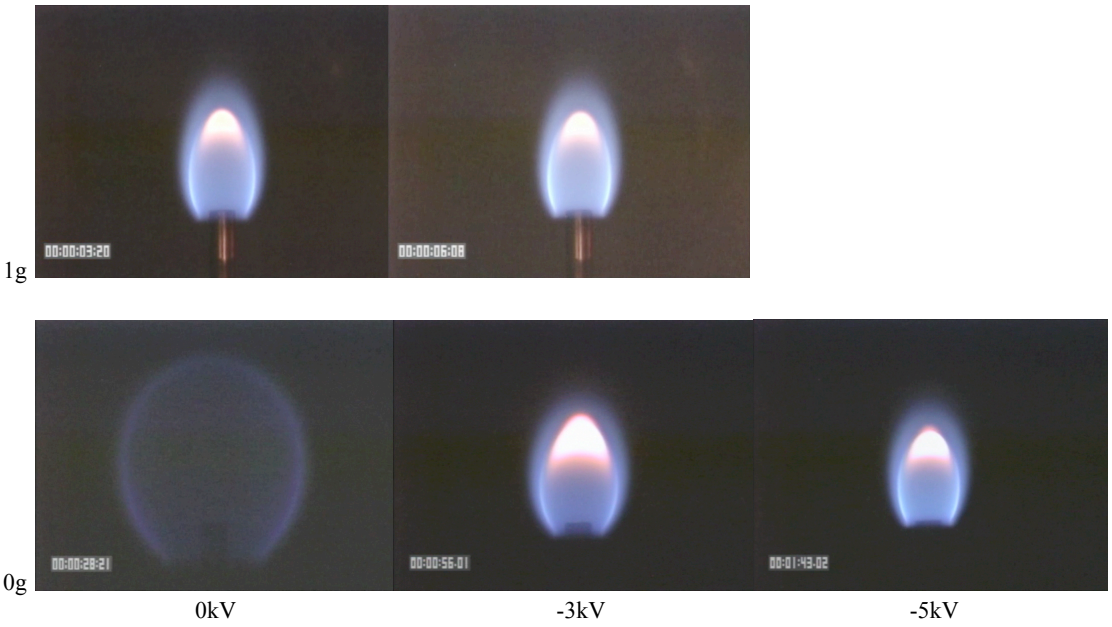

Figure 1.13 – Comparison of 1-g and low-g testing. Testing performed at 24 cm/s. A 5 cm/s coflow is applied in the -3kV case. Mesh to electrode distance is 5 cm.

tially detached and then reattached to the burner. The variations in the flame shape and the liftoff height during the oscillation are reflected in the ion current signal. Because of the competition between buoyancy and the ion-driven wind, we expect these oscillation phenomena to be affected significantly by zero-g conditions at low coflow rates. The ion-induced flow from a negative field in μg acts like the buoyancy-induced flow in 1g to destabilize the flame, while the increased liftoff height allowed enhanced fuel-air mixing, thus stimulating the flame base to propagate back toward the fuel tube. If sufficient fuel-air mixing time (≈100 ms) is available, the flame base can propagate through the stratified mixing layer at the flame speed of a stoichiometric mixture [37].

Testing at lower coflow velocities ranging from 0-5cm/s show dramatic changes in flame shape, as shown in Figure 1.13. Without the influence of large coflow velocities and buoyancy, videos and ion current measurements show the complex interaction between ionization, flame shape, and ion-driven wind. When the field is energized, we can see how the development of the ion wind alters the flow profile, which reshapes flame and intensity of burning, subsequently modifying the strength of the ion wind. In the tests performed, steady state conditions were not achieved.

Building from previous efforts, our numerical approach now includes the effects of combustion chemistry under the influence of an electric field using the commercial software PHOENICS. The goal is to provide additional insight to the complex couplings in our experiment. Additional results and details of the model can be found in reference [35].

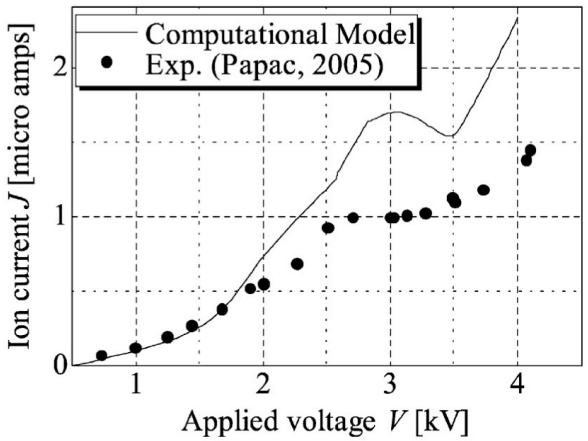

Figure 1.14. Comparison of experimental ion current measurement to numerical calculations

Solving the chemistry and its resulting influence on the electric field helps remove many of the assumptions found in our previous modeling efforts. Based on the geometry in Figure 1.3, we modeled an inverted capillary jet with methane as a fuel, under the influence of an electric field. Figure 1.14 shows a comparison between the experimental ion current measurements and the computed response. The computation recreates the three regions discussed in Figure 1.10, but the lack of quantitative agreement illuminates the sensitivity of kinetic rates and ion mobility. Understanding these coupled parameters will require a system where the chemistry and buoyancy can be decoupled, as in the experiments planned for the ISS. Figure 1.15 shows the computed flowfield at and around saturation, showing its contribution to the change in flame character. At higher applied voltages, velocity vectors show the entrainment of oxygen into the flame zone, evidence of its contribution to creating a partially premixed flame, creating the enhanced ionization region.

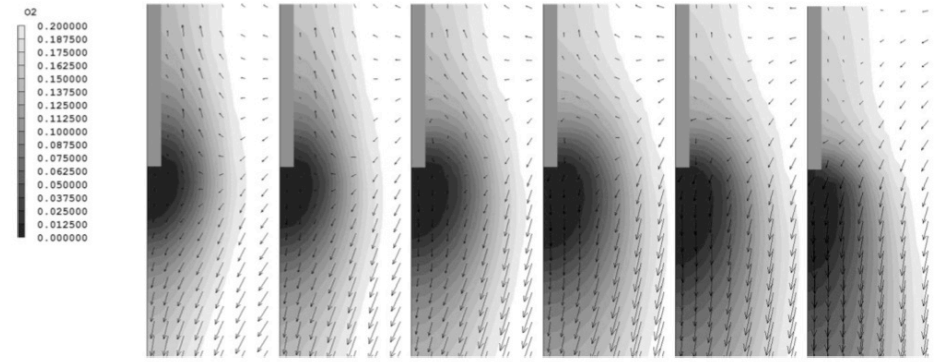

Figure 1.15. Evolution of the velocity field and oxygen distribution and super-saturated region around the flame zone.

The relationship between the VI curve and the flame behavior is a potentially valuable diagnostic tool. As shown in Figure 1.16, the VI curve shape remains fairly constant, but its amplitude changes for different flowrates of methane fuel into the gas jet burner. This result is consistent with the expectation that ion current at saturation scales with total carbon influx into the system [24]. When a different fuel is used, however, the VI curve changes substantially, particularly when the fuel produces soot. An ethylene flame under the influence of an electric field (as in Figure 1.17) appears much different than the methane flame in Figure 1.5. The same kinds of results are discovered when the capillary flame is oriented horizontally rather than vertically in the 1-g earth gravitational field. In the horizontal case, there is no approximate force balance condition and so the ion-driven

wind simply directs the hot flame gases to different locations on the ground plane. A detailed comparison between horizontal and vertical flames and flames of different fuels appeared in [9].

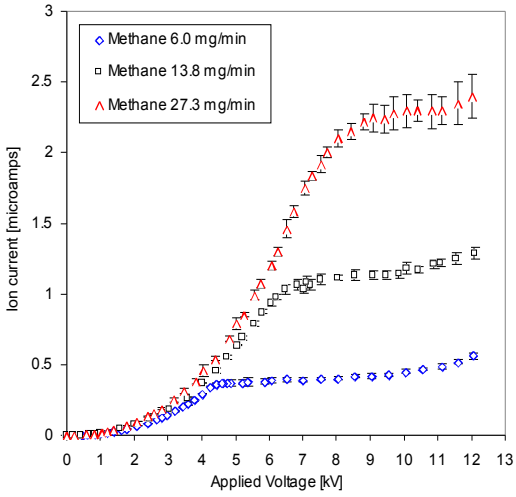

Figure 1.16. Methane VI curves at different flow rates

1.4 Summary of Findings and Open Questions

The above earth gravity experiments have resolved many questions regarding ion driven winds in small diffusion flames, and all of the important experimental conditions and procedures have been established. The ion pathlines and the link between ion driven winds and the flame shape and behavior for small diffusion flames have been identified. Modeling of the electrokinetics along with the fluid dynamics has been successful, thereby providing an analytical tool for understanding the ion wind/flow coupling. The open questions regard the relationship between flame character (e.g., level of partial premixing) and the electric response. In addition, uncertainty remains regarding the chemical versus physical role of ions, and the potential for dynamic manipulation of flames using electric fields.

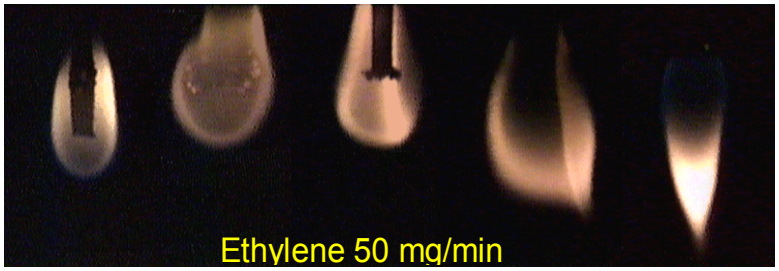

Figure 1.17. Effect of electric field on ethylene flame showing the variation of soot behavior.

The 1-g studies to date did not involve any quantitative analysis of soot because carbon particles complicate the interpretation of electrical properties, but this component of combustion is important to include because electric fields can modify soot formation and burnout [14,40,41]. There is no question that flame soot is electrically charged, as shown in Figure 1.18, but there is a long-standing debate in the combustion community regarding the role of ions in the formation of soot. Essentially, there are the more numerous adherents to the mechanism of soot growth by the addition of neutral hydrocarbon that is exemplified in the work of [42,43] versus those that believe that the addition of ion radical hydrocarbon species are important, as discussed in [23,44,45]. Although recent numerical work has focused primarily on the neutral species approach, there continues to be strong interest in the possible role of ions because there has been no satisfactory ex-

planation from the neutral radical perspective for why the addition of metal ions into a flame reduces soot. If ionic species are important, however, the reason for metal ions suppressing soot is clear since the metal ions will compete for electrons with other species, reducing the formation of potential precursor charged radicals.

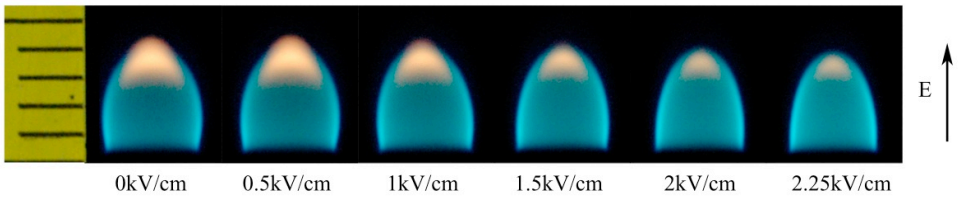

Figure 1.18 An electric field alters the luminosity of soot in an ethylene flame in a coflow.

The E-FIELD Flames experiment provides an opportunity to explore two potential roles of ions in the control of soot. The first is the ionic wind, where local mixing of oxidizer driven by the ion wind can change the residence time of precursor species through the reaction zone and modify soot formation. This mechanism has been demonstrated in 1-g [14], but it has not been quantified because there is a complication of buoyancy. The second is to actually remove ionic species from the flame zone, modifying their time temperature history. This action would directly affect the possible ionic soot growth mechanism. Because the ionic wind effect and the direct ion transport effects are coupled, the tests will not be completely unambiguous, but they will eliminate the complication of buoyant driven flow and thereby provide data that can be analyzed in the context of the soot formation mechanisms to provide insight. The tests then include soot volume fraction measurements as a function of electric field strength (voltage and ion current) at the conditions identified as showing the highest sensitivities to electric field influences.

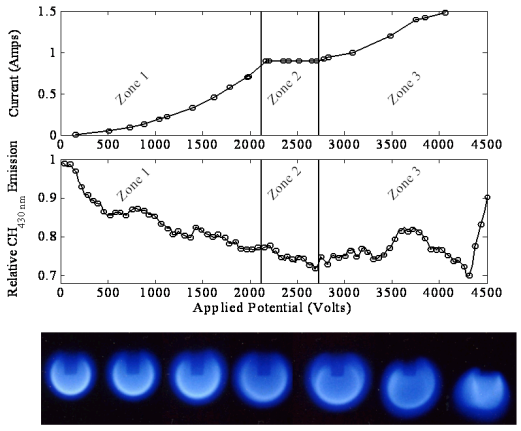

Figure 1.19. Current, CH chemiluminescence, and image of flame as a function of voltage.

Under conditions where the ion current is dominated by soot, thermionic emission from soot provides another tool for electrical flame analysis. Boothman, et al. [24] showed that the thermionic current density (A/cm^2) is given by the Dushman equation,

$$j = BT^2 e^{-e\phi/kT}$$

where B is a universal constant with magnitude between 50 and 60 A/K^{2}cm^2, the e in the exponent is the elementary charge, ϕ is the work function for soot (approx. 4.4 V), and k

is Boltzmann's constant. Knowing the soot volume fraction, the soot temperature, and the ion current, it is then possible to compute the soot surface area and the Sauter mean diameter particle size. For example, using 1 ppmv as a typical soot volume fraction for an ethylene-air diffusion flame, and assuming a soot temperature of 1500K, an ion current of 10 microamp from a flame volume of 5 cc would imply a soot d_{32} (or Sauter Mean Diameter) of 5 nanometers. The same soot volume fraction, with 100 nm soot particles would produce only 0.5 microamps. This sensitivity to surface area can be used to gain further insights into the flame soot growth dynamics.

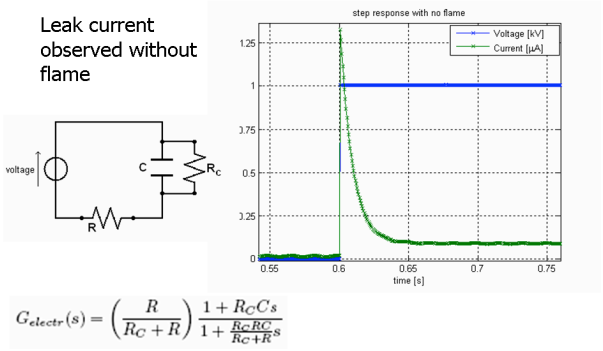

Figure 1.20. Electrical analog model and step response

The above open issues form the basis for our proposed ISS experiment. In particular, we plan to use two burner configurations (primarily the jet flame) with a forcing electrode and controllable high-voltage circuitry to explore: (a) the voltage/current relationship of small diffusion flames, particularly as correlated with the flame luminosity as shown for example in Figure 1.19; (b) the dynamic response of flames to step changes in local electric fields, as shown in Figure 1.20, so that flames can be accurately modeled as electrical elements [29,30,39] for control; (c) changes to flame soot in response to electric fields to determine the relative importance of physical and chemical influences driven by those fields; and (d) the changes in flame behavior near stability limits in response to electric fields to evaluate the potential of local mixing and electrically driven convection to affect those limits. The experimental objectives and details associated with these topics are described in the following sections.

2. E-FIELD FLAMES FLIGHT EXPERIMENT

2.1 Experimental Objectives

The ultimate objective of this experiment is to develop an understanding of the mechanisms of chemi-ionization in flames and to describe the interplay between convective flows driven by those flame ions and their generation rate. With this information it will then be possible to detect and control flame behavior electrically. In 1-g, laminar diffusion flames are often controlled to a large extent by natural convection, and particularly by the rate at which natural convection brings fresh oxidizer to the reaction zone. Hence, the vigor with which combustion proceeds depends on local convection. As described in Section 1, an electric field acting on flame ions produces a body force and convection (analogous to buoyancy) which affects the combustion process. The change in the combustion process can in turn affect the ion production rate, which is responsible for the body force. This coupled interaction is very difficult to measure, study, and understand in 1-g because buoyant forces (of approximately equal magnitude) interfere. In microgravity, there is no such complication and the body force in the flame is associated entirely with the ion-driven wind. 1-g experiments have demonstrated clearly that electrically driven convection can be used to modify the local flow field in a manner that changes combustion behavior. For example, it can stabilize lifted flames or force them to reattach. Electric fields have been seen to change soot formation, though whether solely by residence time effects or their combination with chemical alterations has not been confirmed. In addition, ions can attach to soot particles providing them with enhanced mobility that can be manipulated. Furthermore, the electrical properties of flames provide a measure of their character. For example, non-premixed flames exhibit different relationships between ion production and ion wind forces than do premixed flames. The hydrocarbon fuel, and in particular, the carbon/hydrogen ratio, also affects these interactions. The goal of this project is to clarify and quantify this range of electrical effects and to then demonstrate the electrical manipulation of flame stability and soot in flames using the information obtained.

To accomplish this scientific goal, there are four fundamental experimental objectives, in priority order, using a jet diffusion flame burner and a co-flow diffusion flame burner. The jet flame is the more critical configuration because it has a large 1-g data foundation and it can be more easily modeled as an ion and thermal source. In zero-g, however, it will be primarily driven by ion wind convection (no buoyant contribution and at its low fuel flow rates, the injection momentum dies rapidly with distance from the injector) which may limit its operating range. The co-flow flame allows a forced convection component to provide a wider range of flow conditions (fuel dilution and exit velocity) and a reproducible lifted flame for stability and soot behavior studies:

A) Determine the relationship between electric field voltage and chemi-ion current as functions of total fuel (methane and ethylene) flow rate and the amount of inert (nitrogen) in the fuel.

For the above determination, a low-sooting and highly sooting fuel are included, and the inert weakens the flame sufficiently to permit near-limit conditions at moderate flow velocities, where the effects of electric fields will be most acute. As shown in Figure 1.10, the resulting voltage-current (VI) curve (also known as the voltage current characteristic -- VCC) from these experiments will identify the voltage and current at which the ion current first saturates, the voltage at which the current begins to increase beyond saturation, indicating a change in combustion behavior, and the voltage at which the flame extinguishes. These data can be analyzed further to provide the ion production per carbon atom of fuel flux which describes the flame character (i.e., diffusion to partially premixed), and the ion wind strength for each condition. In addition to their direct interpretative value for calculating ion-driven winds and body forces, these data can also be used in electrokinetic simulations to compute ion mobility values consistent with measured ion currents and to help validate the numerical simulations of other researchers that include ion species and electrical effects in their flame calculations.

B) Obtain the time response of the flame chemiluminescence, luminosity, and the ion current to large step changes in voltage, as functions of total fuel (methane and ethylene) flow rate and amount of inert (nitrogen) added to the fuel stream.

These data provide the dynamic system behavior of the flame. This information comprises the time response of the flame (i.e., its surface area and luminosity) as compared to the time response of the ion current. These timescales can temporally separate the direct chemical effects of electric fields from ion diffusion and ion wind convective forcing. In addition, the system response is required to eventually build flame models suitable for active electrical control, assuming linear behavior over small ranges.

C) Evaluate and manipulate sooting behavior (i.e., soot volume fraction and location of luminous soot) in relation to the electric field voltage and chemi-ion current as functions of total fuel (methane and ethylene) flow rate and amount of inert (nitrogen) added to the fuel stream.

The interaction between soot and electric fields is very complex because it combines the direct influence of electric fields on the chemistry, the ion wind effects on residence time and mixing, and the electric forces on the charged soot particles themselves. The zero-gravity environment, using the combination of the jet diffusion flame and the co-flow flame provides a wide range of conditions where these different influences can be allowed to dominate individually. For example, the forced convection environment of the co-flow burner will minimize the influence of the axial ion-driven wind, which helps to distinguish the direct electrical effects on ion chemistry in soot formation. In addition to demonstrating the direct control of soot behavior by electric fields, separating the influences can help distinguish between neutral molecule addition mechanisms of soot formation and those that presume the importance of ionic species. For example, changing the strength and polarity of the electric field can change the availability of ion precursors, and electric convection can manipulate reactants' time/temperature history. In addition, charges will accumulate onto soot, and the electric field can then act directly on the soot particles to change their residence time and path through the flame.

D) Use the variation of the chemi-ion current as a function of applied voltage to characterize the combustion behavior of near-limit lifted flames and use the associated ion-driven wind to stabilize or reattach these flames.

Because the chemi-ion current per unit flame area can be used as an indicator of flame strength, its measure (both average and fluctuating properties) with low electric field voltage can be used to detect flames approaching their limit condition. By adjusting the electric field, 1-g studies indicate that an ion driven wind can be used to reduce the lift-off height and stabilize the flame. This is an example of open loop electrical flame sensing, analysis, and control.

2.2 Approach

The specific experimental objectives of the electric field experiments all examine the potential for electric fields to distinguish and manipulate combustion behavior of laminar diffusion flames, particularly with regards to stability and extinction limits and soot formation and burnout. As described in Section 1, our 1-g studies have shown that small gas jet diffusion flames can be used to study a wide range of electric field/flame ion interactions, particularly as regards the changes to the flames that result from ion driven winds. These flames are compact (allowing complete optical visualization) and require very low flow rates of fuel (on the order of 30 sccm) which makes them well-suited to the CIR experiment environment. The E-FIELD Flames experiment can also take advantage of the co-flow burner that is proposed for the CLD Flame component of the ACME flight experiments. Like the gas jet diffusion flame, the co-flow burner uses very small amounts of fuel, but unlike the jet flame, the burner isolates the diffusion flame sheet from the influence of the static ambient gas with a co-flowing gas stream. The co-flow configuration allows two important aspects of electric field/flame interaction to be studied. First, the effects of the electric field on the lifted co-flow flame can be examined. There is evidence in the literature that electric fields increase flame resistance to lifting, though the liftoff height itself may not change substantially [46,47]. It is likely that this effect is related to the ion driven wind because the lifted flames are sufficiently near their combustion limit to respond to relatively small forcing. This influence can be quantified using the co-flow burner. There is a controversy in the literature regarding the importance of ion driven winds in the liftoff behavior relative to the chemical effects. The controversy cannot be resolved easily in 1-g because buoyancy confounds the flowfield. Recent experiments in our 1-g laboratory confirm that the co-flow burner exhibits some significantly different electric field/flame

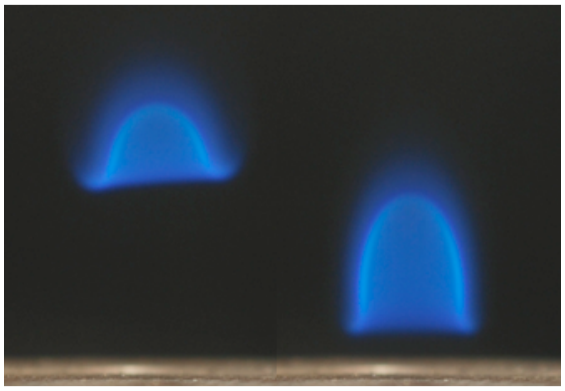

Figure 2.1 Effect of electric field on liftoff in a coflow burner; the positive mesh field produces reattachment.

interactions from the jet diffusion flame. Figure 2.1 shows a typical methane co-flow without and with the electric field.

In addition to controlled lifted flame ion current measurements, in the slightly lifted (but not near-limit) flame conditions, the effect of the electric field on sooting behavior can be measured. As mentioned earlier, there remains some question regarding the role of ionic species in soot formation, and by using the co-flow burner configuration, we will be able to affect the flame electrically without distorting the flame with the ion-driven wind as necessarily occurs in the simple gas jet diffusion flame.

The detailed list of flame conditions to be studied is included in Section 3 and in the Appendix (e.g., test matrix of conditions). The basic variations in the tests, however, are in the burner type (simple gas jet and co-flow), the fuel type (methane and ethylene), and in the level of inert (nitrogen) dilution of the fuel. The co-flow gas will be air with molar composition of 21% O_2 and 79% N_2. If additional fuel gas combinations and oxidizer is available (e.g., CO_2 diluted fuel), then additional experiments can be run following the same procedures outlined below.

The schematic approach of the E-FIELD Flames experiment is shown in Figure 2.2. The concept is to ground the burner to the chamber through a safety bleed resistor-capacitor pair, and to install an electrically active mesh electrode downstream of the burner mouth. A tentative electrical configuration is shown in Figure 2.3. These figures show that the high voltage connection is attached to the mesh, with the ion current measurement being made across a shunt resistor connected between the burner and the low potential (relative to system ground) side of the high voltage source. This configuration requires that the burner be electrically isolated from the rest of the chamber, but the electrical isolation (in terms of breakdown potential resistance) can be relatively modest since the potential difference across the shunt resistor will not be significant during normal operation (e.g., on the order of 1 V for a 100 kΩ shunt resistor and 0.1 microamp chemi-ion current). The potential of the mesh electrode can be either positive or negative, with a steady voltage or with a time-varying but unipolar voltage (including a step change) to examine the flame's steady state response and time response to such changes. The goal of the design is to eliminate any leakage current so that all current flowing through the shunt resistor is the result of chemi-ionization in the flame. In 1-g studies, there have been cases where soot formed on the burner acts as a weak electron emitter (see, e.g., Figure 1.17). Even in this situation, the leak current is small (less than 5%), but it is preferable to have a mechanism for removing soot buildup on the burner should it occur. The removal can be manual, or non-lifted, non-sooting flame conditions can be used to burn the soot from the burner tip *in situ*.

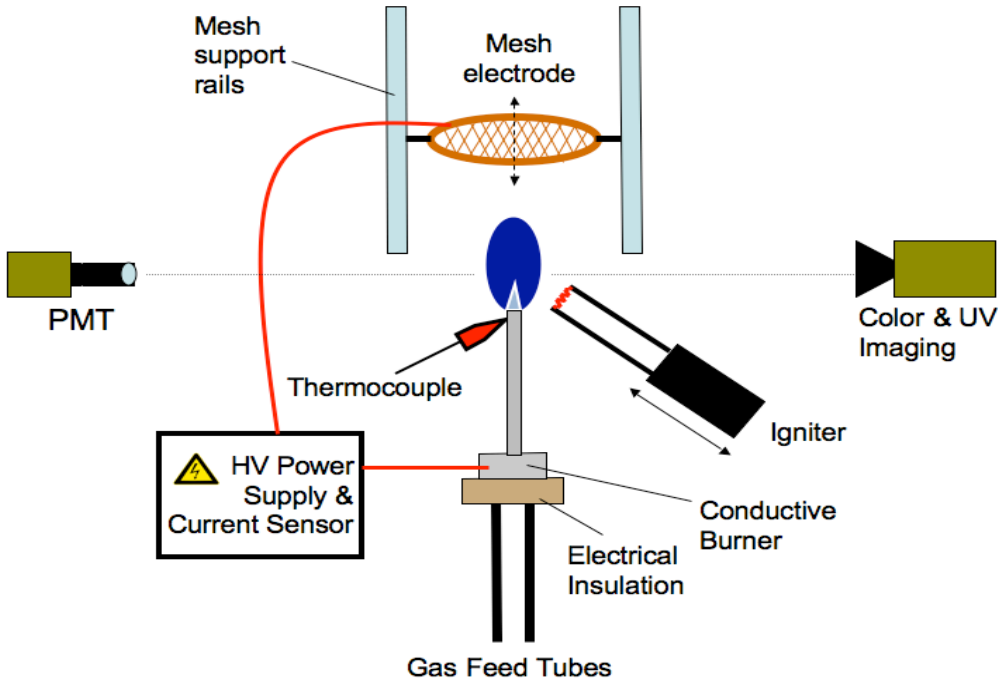

Figure 2.2. Overall schematic of the E-FIELD experiment in the CIR. Shown is the gas jet burner, but the co-flow configuration would be similar with the substitution of the burner.

The data to be recorded include the applied voltage, the ion current, the flame broadband luminosity, the spatially integrated CH* luminosity, flame images of OH* and visible light showing the flame shape as a function of electric potential and flame shape changes during transients in the electric field. In addition, a measurement of temperature in and near the flame can monitor the thermal field as a function of the electric field conditions.

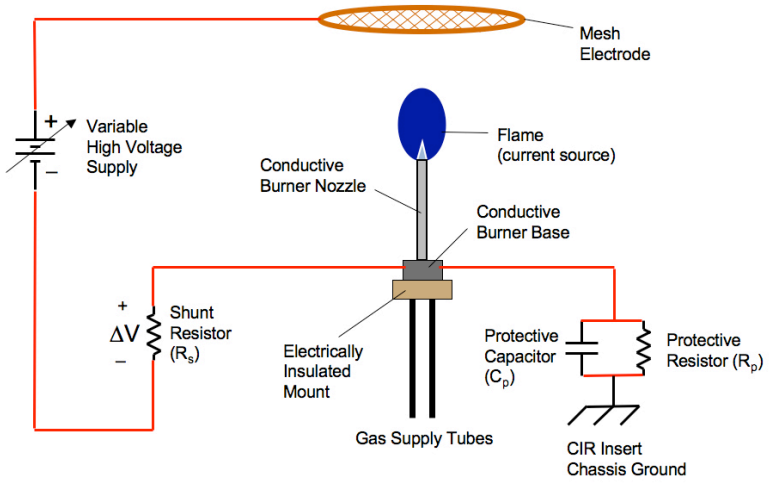

Figure 2.3. Electrical schematic for E-FIELD experiment.

We envision that the measurement could consist of a schlieren image in non-sooting conditions (desired) and soot pyrometry in the sooting regions. A thermal sensor (e.g., thermocouple) near the burner tip could determine if heat from the flame is diffusing back to the burner and possibly affecting the exit gas temperature and flame stability. This

effect has been found to be significant for slightly lifted small co-flow flames, particularly near their stability limit [48]. Pyrometry on the simple gas jet tube could give similar information when the view of the fuel tube is unobstructed.

2.3 Science Data End Products

Having defined the objectives and the experimental approach of this investigation it is now possible to define a group of final data products that is sufficient to fulfill each objective. Final data products are the graphs, analyses, and figures that will be reported in the archival literature. These final data products are referred to as the "Science Data End Products" (SDEP). The science requirements and the experiment success criteria described below are developed from this list of SDEP. Before defining the SDEP, we review briefly the independent (or manipulated) variables and the dependent (or responding) variables that will form the raw data from the experiment. A description of the SDEP then follows.

2.3.1 Independent Variables

Co-flow condition (i.e., burner type) – two types of burners are used. A simple gas jet burner that has no co-flowing gas and a co-flow burner that includes an annular sheet of oxidizer flow around the inner circular cross-section fuel jet. The co-flow condition affects the relative importance of the ion-driven wind relative to the forced convection in controlling flame behavior and can produce a steady lifted flame. Both burners have a large 1-g data foundation; the former with and without electric fields (e.g., [8,9,33]) and the latter without electrical effects but with comprehensive modeling and detailed diagnostics (e.g., [49-51]). There are two gas jet flame burners (without coflow) to be used, the only difference being their diameter. One matches the current 1-g jet flame studies and the other (desired) matches the fuel tube of the co-flow burner so that direct comparisons can be made with regard to any changes in entrainment affected by the co-flow annulus. We will also run experiments (desired) using the co-flow burner but without any co-flowing gas because entrainment effects will be different for flames in this configuration compared to the simple gas-jet flames even when the fuel tube has the same diameter.

Fuel type – two fuels: methane and ethylene are used. The former is a low sooting fuel with a low C/H ratio of 0.25. This fuel is predicted to produce a clean burning flame with relatively low ion production and ion driven wind strength. It also has the broadest earth gravity data set associated with electrical aspects of flames. Ethylene is well-known to have high sooting tendencies, with a C/H ratio of 0.5. Its higher carbon content also produces higher ion production and larger potential for ion driven winds. This fuel will allow broad exploration of the potential for electric fields to control flame soot. Our earth gravity studies confirm that the two proposed fuels behave differently (e.g., [9]). These two fuels are also those being proposed for the CLD Flame experiment (with the same coflow of air) allowing comparisons with flames not influenced by electric fields.

Total flow rate of fuel (including inert) – the total fuel flow rate sets the exit jet velocity and thereby the relative importance between jet momentum and ion driven convection. The electrical effects will dominate under conditions of low ejection momentum. However, in the co-flow burner, even when the exit jet velocity is fairly high the momentum match between the fuel stream and the co-flow sheath means that the cross flow momentum can be low, so radial electrical influences may still be important. This total flow rate parameter also controls the liftoff height of the flame.

Dilution with inert (nitrogen) of fuel – ion production mechanisms predict higher concentrations of chemi-ions under conditions that create higher concentrations of oxygen radical. In a premixed flame, this variable can be manipulated by adjusting the equivalence ratio and reducing the flame temperature. In a simple non-premixed flame, however, the reaction zone coincides with the stoichiometric condition and so dilution of the fuel with an inert can serve this purpose. In addition, dilution with an inert can weaken the flame by reducing the heat release rate per unit of fuel inlet flow mass. At their limit, these flames are most susceptible to the forcing flows and entrainment that can be driven by flame ions.

Voltage (V), polarity, and distance between electrodes – as shown in Section 1, the ion wind body force is a direct function of electric field strength and ion concentration. The electric field strength is a function of voltage and distance between the electrodes, as well as any space charge effects. Switching the polarity of the voltage source is important for changing the role of charge carriers during electric field forcing of flames. The direction of the ion driven wind does not always change dramatically with electric field polarity because the wind generally flows in the direction of the most distant electrode. This interesting uni-directionality occurs because the active ion polarity switches to accommodate the change in field. That is, the ion wind is driven either by negative ions produced by electron attachment to neutrals beyond the flame or H_3O^+ ions surviving beyond the flame. Because their distance to the electrode is generally short, the oppositely charged ions or electrons do not create a significant opposing wind. This behavior may not hold when the flame is lifted a substantial distance from the burner surface. Even if the wind direction does not change, however, its strength changes substantially because of the relative concentration and mobility differences between the ion species responsible. In addition, direct effects on charged species within the reaction zone will be different for different polarities. We have observed clear indications of these directional wind changes in microgravity from our recent results obtained in the 2.2 s drop tower.

2.3.2 Dependent Variables

Chemi-ion current (I) – the ion current is a primary indicator of chemi-ionization in the flame, and varies depending on flame character, reaction zone size, and combustion intensity (heat release rate). This is a global measurement of current flowing through the shunt resistor. A current measurement without the flame present provides the baseline leak current and ensures that there is no corona discharge or conducting pathway contributing to the measured current. Our 1-g studies show that the experimental configuration

described previously has essentially zero leakage current. Excessive leakage current with no flame may indicate significant soot buildup and be an indicator of cleaning required.

Flame shape and size – in order to determine the effects of ion wind on the reaction zone, images of the flame are needed. Images of the flame reveal the flame area, provide evidence of combustion intensity, identify locations of soot formation, and show how the ion wind (local convection) changes the flame shape for the various input flame parameters and electric field strength. These line-of-sight integrated images will be Abel-inverted to provide the true reaction interface size and location. Color video images provide information regarding the location of luminous soot and the visible reaction zone interface. UV images with a filter for OH* provide a sharp determination of the reaction zone. The images of CH* chemiluminescence (desired) can be related to the local rate of heat release, which also correlates to chemi-ion production. This last measurement is "desired" because the combination of the visible images and the OH* images are expected to provide approximately equivalent information.

Soot volume fraction – quantitative evaluation of the effects of electric fields on soot formation, transport, and burnout require this information over the flame zone. We expect this measurement to be made by extinction followed by Abel deconvolution. Soot volume fraction is also needed to estimate mean soot particle size from the Dushman equation as described at the end of Section 1.

Spatially integrated luminosity – Broad spectrum flame luminosity, which includes the chemiluminescence and soot radiation collected over a large solid angle (not imaging) provides a rapid global response variable of how the flame reacts to changes in the electric field. Laboratory studies (see, for example, Figure 1.5 and 1.19) have shown that this luminosity signal can be correlated to flame appearance and ion current.

Spatially integrated chemiluminescence (CH)* – CH* chemiluminescence can be related to heat release rate and its collection over a broad solid angle (not imaging) provides a rapid response variable of how the flame reacts to changes in the electric field. Normal gravity studies have shown that this chemiluminescence signal can be correlated to flame appearance and ion current and can be used as a sensor in controlling and monitoring combustion [30].

Burner temperature (desired) – The temperature of the burner surface, provides the inlet thermal boundary condition of the flow. This temperature is important to show how much the flame interacts thermally with the burner. The burner/flame interaction has been shown to affect flame stability for very small jet flames [48] and it can also change the inlet conditions for coflow flames when the lift-off height is very small. This measurement is desired because it is likely that the burner temperature effect is much more significant in 1-g where a rising buoyant plume from off the burner can interact at the flame base. In zero-g, this will not occur and so the effect involves only thermal aspects.

Gas temperature in and near the flame (desired) -- Measuring the temperature field between the flame and the electrode shows the shape and structure of the thermal plume. In

the jet diffusion flame, 1-g experiments show that this boundary coincides with that of the ion-driven wind region. Schlieren imaging (e.g., as in Figure 1.5) provides an indication of the boundary and distributed temperatures (such as would be provided by shadow deconvolution and soot pyrometry in sooting regions). Unfortunately, laboratory studies have shown that silicon-carbide thin filaments in the flame change the electrical behavior substantially, so we cannot use thin filament pyrometry in soot free regions. The thermal information is valuable however, as it allows the current density, the ion mobility, and thereby the electric body force, to be calculated most accurately. In laboratory studies, for example, we have seen evidence of substantial differences in ion mobility and ion wind depending on the thermal field the ions traverse. In the case of the co-flow flame, the thermal plume is governed by a combination of the ion driven wind and the forced convective flow. Comparison between the temperature fields with and without the electric field can be used to estimate the ion driven wind contribution in this case, which helps resolve the controversy alluded to earlier regarding the relative importance of chemical and physical effects in electric field resistance to liftoff. These results also allow comparison with 1-g studies of electric control of heat transfer in flames, as discussed in 1-g by Sandhu and Weinberg [31].

Section 1 shows many examples of the kinds of SDEP figures (except that they are at 1-g) that will result from this study. The following subsections outline in more detail some specific data end products associated with each objective, along with the significance of these products. After the lists, Table 2.1 summarizes the measurements and their role in meeting the experimental objectives.

2.3.3. SDEP (Objective A) – steady state chemi-ionizaton in flames

A typical steady-state voltage-current (VI), also known as the voltage-current-characteristic (VCC), curve is shown in Figure 1.10 for a gas jet flame and in Figure 1.11 for a co-flow flame. Our 1-g studies have shown that the important transitions in the VI curve are representative of the flame character (e.g., diffusion flame versus partially premixed flame), including the onset of saturation, the saturation current at the first plateau, the length of the saturation plateau, the onset voltage for additional ion production, and the voltage blowout limit. SDEP include, therefore, typical VI curves for different fuels, flow rates, and dilutions. A representative set of curves is shown in Figure 1.16, where the VI results shown for different fuel flow rates demonstrate that the saturation current scales approximately with carbon atom influx into the flame, but that a secondary increase in current does not occur. Similar curves will be obtained in the zero-g environment.

In addition to typical VI traces, the first plateau for each flame condition provides the saturation current per fuel carbon. The set of tests then provide saturation current as a function of inert dilution for two fuels and two burner types. Such results can be compared with the 1-g findings of Boothman and Weinberg [24], who found little effect of dilution. Figure 2.4 is from our 1-g efforts and it shows the result of a similar interpretative approach for the data. In this case the jet diffusion flame is being diluted with air, rather than an inert. There is a dramatic transition of saturation current (J_s) per fuel car-

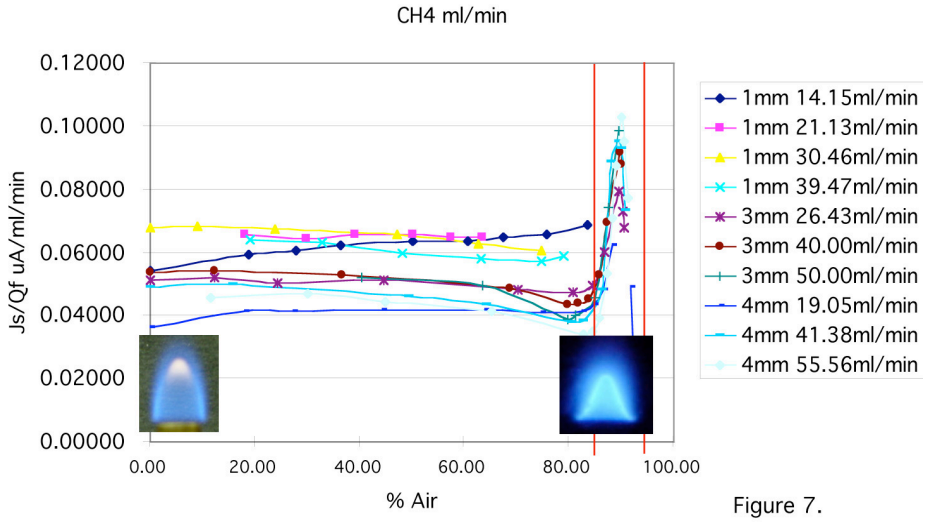

Figure 7.

Figure 2.4. Change in saturation current per unit of fuel carbon as a function of dilution of the fuel for various flow rates and burner diameters. The images show how the flame appearance changes with dilution.

bon flux (Q_f) behavior with dilution of the fuel. The transition results, apparently, from fundamental changes in the flame character as the air dilution increases beyond a critical value. It is interesting to note that standard gas analysis by flame ionization detection relies on the fact that J_s/Q_f is nearly constant, as shown for the low dilution regime.

In addition to the saturation current per carbon atom influx, the voltage at which additional ion production occurs, as a function of fuel flow rate and inert dilution for the two fuels and two burners, shows when the ion wind induced entrainment of additional oxidizer into the flame zone breaks down the purely diffusion flame character. The voltage at which the flame blows out, again as a function of fuel flow rate for different inert dilution for the two fuels and two burner types, sets the limit of operation for the electric field manipulation of flames, and also provides the maximum ion current condition achievable.

Flame images, both natural luminosity and filtered CH* (desired) after Abel deconvolution, for different fuels, flow rates, and dilutions show the qualitative sooting tendency and the location of the soot relative to the primary reaction zone; CH* (desired) and OH* images also provide the flame surface area and a semi-quantitative measure of combustion intensity. Schlieren images (desired, e.g., Figure 1.5) identify the thermal plume and provide information for approximating variation in ion mobility. The images can also be compared to steady electrokinetic calculations as shown in Figure 1.9. The combination of flame images and saturation currents can be plotted as saturation current per unit flame area, which is characteristic of flame robustness.

Specific SDEP associated with this objective will include:

1) Typical plots of voltage versus ion current (VI) for gas-jet and co-flow flames, for ethylene and methane as fuel
2) Typical flame images associated with the important transition points in the VI curves

3) Empirical model of saturation current as a function of inert concentration in the fuel for different fuels, for gas-jet and co-flow flames
4) Voltage (ion-wind) and current at the onset of enhanced ion production as a function of the inert concentration in the fuel, for gas-jet and co-flow flames
5) Voltage (ion wind) and current at flame blowoff as a function of the inert concentration in the fuel for gas-jet and co-flow flames
6) Saturation ion current per unit fuel carbon as a function of flow rate and inert percentage
7) Flame luminosity (mean and RMS for CH* and broadband visible) as a function of voltage and ion current, for gas-jet and co-flow flames
8) Saturation current as a function of flame area
9) Thermal plume shape as a function of electric field forcing (desired)

2.3.4. SDEP (Objective B) – time response of flames to electric forcing

Time resolved measurements after step changes in voltage are necessary to determine the temporal response of flames to electric forcing. In particular, the time resolved ion current, as shown in Figure 1.20, provides the ion flux timescale given by any time delay beyond that of the natural capacitive decay time for the experimental apparatus. In 1-g studies, the system electrical response is dominated by the slow capacitive timescale, which may also be the case in microgravity. Time resolved measurements of spatially integrated luminosity (including soot) and CH* filtered light from the flame in concert with the ion current measurement monitor changes in the flame behavior for comparison with the capacitive timescale. As shown in Figure 1.19, the steady-state flame luminosity changes with electric field. The timescale of this change is a combination of any rapid chemi-ion transport effects and the slower convective timescale effects arising from changes in the ion driven wind. Computational and experimental studies show that at 1-g, the convective effects can require hundreds of milliseconds to first influence the flame and a longer time to reach quasi-steady state (e.g., [52]). The longer secondary timescale response appears to result from the development of a quasi-steady convective flowfield driven by ions. Our recent drop tower microgravity tests show that the time response behavior is significantly different in zero-g, with less dependence on the timescales associated with buoyant flows. In addition, by comparing the broadband luminosity response to that of the CH*, it will be possible to separate the soot development timescale from the ion flux timescale and from the fluid/chemical timescale in the electrically driven flame. Luminosity timescale comparisons between different flame conditions will characterize these dynamics. Equally important, the time response results will allow control modeling of flames for eventual use in combustion control.

1) Typical time resolved ion current after step changes in voltage
2) Typical time resolved luminosity after step changes in voltage
3) Electrical time constant of the flame as a function of inert concentration in the fuel and flow rate, for gas-jet and co-flow flames
4) Luminosity time constant (both broadband and CH*) of the flame as a function of inert concentration in the fuel and flow rate, for gas-jet and co-flow flames
5) Equivalent RC circuit for gas-jet and co-flow flames

2.3.5. SDEP (Objective C) – electric field influence on sooting behavior

It is well-known that electric fields can have a dramatic effect on soot in flames [14,41,53], but the relative role of direct chemical effects compared with ion driven wind convective effects remains unclear. The data associated with this objective comprise soot volume fraction, soot temperature, color video flame images, CH* images (desired), and ion currents for steady state conditions over a range of voltages. In particular, we will be looking for the critical voltage (which can be related to ion driven wind and ion transport) at which sooting is suppressed as a function of inert dilution of the fuel. The conditions showing substantial changes with electric field will be identified from the data obtained in Objective A and B. A comparison between the results in the gas jet diffusion flame and the co-flow flame can distinguish the relative roles of ion-driven convection versus chemistry in this process.

1) Average soot volume fraction as a function of ion wind, for different inert levels in fuel, for gas-jet and co-flow flames
2) Typical images showing location and temperature of soot for different ion wind conditions (e.g., electric field polarity), for gas-jet and co-flow flames
3) Soot mean size based on soot volume fraction and the total ion current from the flame via the Dushman equation
4) Spatially resolved soot volume fraction at transition conditions as the ion wind suppresses soot
5) Voltage (ion current) at which soot is suppressed for different levels of inert in fuel, for gas-jet and co-flow flames

2.3.6. SDEP (Objective D) – electric field sensing and control of near-limit flames

There are two main elements to this objective. One is to use the ion current as a sensor for identifying the incipient extinguishment of lifted flames and the other is to increase the flame's resistance to blowoff. Diffusion flames near their blowoff limit in 1-g generally exhibit an unstable fluctuation just before extinguishing. The fluctuation appears in the chemiluminescence, in the location of the flame base (liftoff height), and in the chemi-ion current. The data products are, therefore, the mean and RMS ion current at low voltages as functions of fuel flow rate and inert dilution in the fuel. Near limit flames are identified from data in Objective A where the fuel flow rate and the inert concentration are increased to flame extinguishment. Extended time at microgravity is necessary for these experiments because the blowoff process is stochastic and can involve long periods of fluctuation.

The second element of this objective is open-loop control, using the ion driven wind to restabilize near-limit co-flow flames. This phenomenon has been observed by Won, et al. [46,47] as manifested by a resistance to flame lifting. They find, for example, that a higher velocity is needed to maintain a fixed liftoff height when the flame is under the influence of an electric field. There is a question, however, whether the effect is simply due to an additive ion wind to the jet flow or if there is a more subtle influence of local

mixing that changes the flame propagation velocity. By measuring the liftoff height, the fuel flow rate, and the ion current, it is possible to distinguish these influences. For example, a substantial change in liftoff height accompanied by a modest ion wind (determined from the ion current and flame surface area) relative to the flow rate would suggest a local mixing effect whereas when a larger ion wind is involved we would likely identify a broader mean flowfield influence. Extended microgravity conditions are necessary to establish the relationship between electric fields and liftoff height behavior because the flame's liftoff height can oscillate slowly for several cycles before it either blows off or reattaches [54].

1) Typical curves of time resolved ion current and luminosity of near limit flames
2) Typical sequence of images of flame from its near limit condition after electric field is activated
3) Mean and RMS ion current and luminosity of near limit flames as a function of inert concentration in the fuel, for gas-jet and co-flow flames, with and without electric field
4) Liftoff height of flames versus voltage (ion wind) as a function of inert concentration in the fuel and fuel flow rate, for co-flow flames (we expect gas jet flames to be too long for useful liftoff height studies in microgravity and so they are not included for this task)
5) Ion driven wind velocity in the region of the lifted flame base determined from ion current measurements and estimates of ion mobility based on the temperature field

2.4 Knowledge to be Gained

As is detailed more completely above, the knowledge expectation is to develop a chemical and physical understanding of flame ion production and the potential to then use this information to control the flame both via modification of the local chemistry near extinction limits and through changes in the local convection using the ion driven wind. Hence, we begin by mapping the electrical response of a wide range of flames and then concentrate on particular conditions of interest, particularly those near limit and transition conditions in diffusion flames. For example, the saturated ion current is a characteristic of the carbon flux into the flame so long as the flame character does not change. As the ion driven wind begins to influence the reaction zone, the saturation current can change dramatically. We are interested in the flame condition near this transition. Similarly, a lifted diffusion flame near its blowoff condition is sensitive to mixing at the flame anchor point. Electric fields acting on such flames can exert large influence because they can affect the local mixing behavior. We are interested, therefore, in these near-limit flame conditions. Finally, the role of electric fields on soot formation will be most dramatic under conditions where the ion driven wind has the largest influence on flow residence time (or on ion residence time, if chemical effects are found important) in sooting flames.

The explanation of the knowledge gaps associated with electric field effects in diffusion flames have been described in the foregoing sections. It is worth making some general statements in this regard, however, to summarize. The goal of this zero-gravity study is

to understand chemi-ionization behavior and the resulting ion driven winds sufficiently well so that electrical properties of flames can be used to characterize (by monitoring ion current) and control them (via direct chemical or local convective influences). Electric field effects on flames have been documented for decades (even centuries), but flames in 1-g all include buoyancy influences. For flames near transitions and limits, buoyant influences always confound any understanding of the role of ion driven winds in using electric fields to characterize and manipulate flames. The proposed study removes this confounding influence and allows definitive measurement and analysis of the electric field effects on sooting, saturation current, and dilution on coflow and jet diffusion flames.

TABLE 2.1. Summary of Measurements and Value Toward Objectives

Measurement	Flame properties	Analysis Value toward Objectives
Ion current	Chemi-ion production	Objective A – identify saturation current and onset of enhanced chemi-ionization in flames; Objective B – measure response time of flame as an electrical element; Objective C – evaluate ion wind effect on soot residence time; Objective D – monitor ion current as a sensor for near-limit flame stability.
Color video images of the flame	Reaction zone location; soot location; flame size and shape; liftoff height	Objective A – find ion current per unit flame area and evaluate flame structure when ion current enhancement occurs; Objective B – compare electric time response to flame shape response time; Objective C – relate electric field condition to soot location in flame; Objective D – measure flame liftoff height and near-limit flame behavior.
Unfiltered non-imaged light from flame	Qualitative measure of soot and reaction intensity	Objective A – relate steady state ion current to flame luminosity; Objective B – relate time response of ion current to that for luminosity; Objective C – measure overall sooting level; Objective D – monitor near limit flame luminosity.
Filtered OH* video of the flame	Reaction interface area	Same as for color video except improved quantitative result for reaction location
Filtered CH* non-imaged light from flame	Measure of reaction intensity	Same as for unfiltered total light except improved results related to heat release rather than overall flame brightness which might be dominated by soot.
Spatially resolved soot volume fraction	Location of soot formation, growth, and burnout	Objective C – quantitative information regarding the effects of electric fields on soot formation; comparing results for co-flow burner and jet diffusion burner provides insight regarding chemical versus physical influences of ion flux
Burner temperature	Heat loss from flame to burner	Objectives A,B,C,D – measures the role of heat interaction with burners and on the liftoff height in near-limit flames; provides thermal boundary condition for numerical analyses
Temperature field above burner, non-sooting and sooting (desired)	Location of thermal field associated with the heat release region	Objectives A,B,C,D – Determines the path of the ion driven wind; allows improved estimates of ion mobility; measures changes in heat transport due to ion driven winds; allows estimate of soot mean size via the Dushman equation.

2.5 Justification for Extended-Duration Microgravity

As described in the Background and Overview (Section 1.1), electric field effects and buoyancy effects have been found to be of the same order of magnitude. In addition, in some cases, raising the flame temperature will increase the O atom concentration, thereby increasing the ion production rate and increasing the response to an electric field. At the same time, increasing temperature increases the buoyancy effect, making it difficult to separate ion wind effects from buoyancy. In the zero-g environment, it will be possible to eliminate the buoyancy confusion and develop sufficient understanding to predict the response of flames to electric fields under all conditions. For electrically driven flames, microgravity is also necessary to create conditions that produce symmetric flames suitable for Abel inversion and steady-state analysis. While in general natural convection can enhance symmetry relative to non-buoyant flames, a flame at 1-g in an electric wind experiences buoyancy as a disruptive influence on symmetry. Even when buoyancy effects can be minimized, we have found that there are periodic disturbances that disrupt the ideal symmetry. Highly symmetric conditions of extended microgravity are also useful for numerically simulating these various effects by our electrokinetic model or more comprehensively by others.

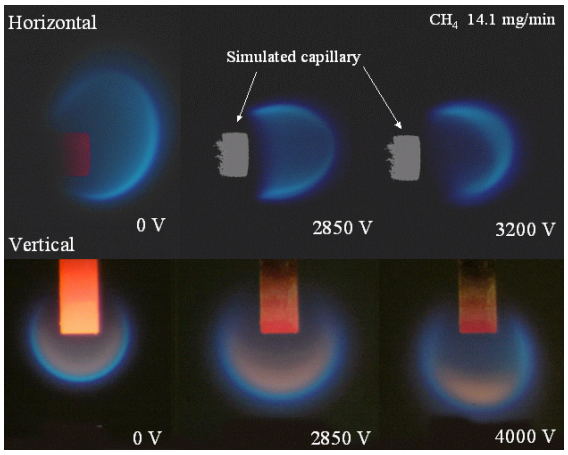

Figure 2.6. Effect of orientation on combustion of 1.8 mm jet diffusion flames in 1-g.

Finally, in order to fully evaluate the potential for control, it is important to examine the effects separately. An example of the importance of microgravity for the electric field effects studies is shown in Figure 2.6. This figure compares the capillary flame used for 1-g experiments (which has some similarities to the jet-flame companion study) when it is oriented vertically to when it is oriented horizontally relative to gravity. These flames behave differently in shape, size, and ion production demonstrating the substantial influence played by buoyancy even in the relatively small capillary flames. Gravity effects in the co-flow flames have been described in the SRD for the CLD Flame experiment, and the same influences will be important when we apply electric fields. Only in extended microgravity will it be possible to separate the ion driven wind effects from buoyant wind effects.

Extended run times are crucial for all of the studies because the timescales involved extend beyond drop tower capabilities and the microgravity quality required for symmetry and stability exceeds aircraft microgravity. The electric-field flame interaction tests carried out in the NASA Glenn 2.2 Second Drop Tower tests by Yuan and Hegde [55] showed that the flame did not appear to reach steady state during the 2.2 sec. drop. Furthermore, their results showed substantial differences in flame shape between cases

thermore, their results showed substantial differences in flame shape between cases where the electric field was activated half-way through the drop and at the beginning of the drop, again suggesting that steady state was not achieved. Although, we varied the range of tests performed at the Drop Tower, our research group encountered similar obstacles. Drop times were insufficient to achieve a steady flame after voltage changes in one direction. Additionally, we were unable to capture the removal of soot from the ignition event and the subsequent response of the flame to the electric field. Furthermore, testing has shown path dependence in the response time of the flame when subjected to step voltages of varying polarities. Properly mapping the steady-state ion current as a function of applied voltage requires that the flame stabilize at each applied voltage. Generally speaking, the timescale of flame property changes (which includes chemi-ionization) is dominated by convection (length scale/velocity), which is on the order of 0.1 second. In order to ensure quasi-steady conditions of the VI characteristics for a single flame configuration with some fidelity (e.g., 50 steps of 200 V each, with 2 seconds between steps for settling after the change), requires more than 100 seconds of continuous high quality microgravity. Each condition and voltage cannot be run individually (i.e, with separate drop tests) because the 2 second settling time requires that the flame begin at a settled initial condition before taking another relatively small voltage step. If we tried to step to the initial condition, allow settling, take the base measurement, then step the voltage and again wait the required settling time, we would exceed 5 seconds for each test in nearly all cases. To run a return voltage sweep to examine hysteresis might take a further 100 seconds. Furthermore, these times are based on 1-g results which under low ion wind conditions are likely to be faster than occurs in zero-gravity since their the convective timescales can be substantially smaller (under low electric field forcing conditions, for example).

Understanding the electric field effects on soot is another area that requires high quality zero gravity timescales longer than is available in drop towers. A variety of zero gravity diffusion flame experience has shown that quasi-steady soot formation requires many seconds [22,56,57]. The long duration is necessary since we are exploring the relative importance of residence time modification of these processes in these flames. In addition, as mentioned above, instabilities and extinction behavior in near-limit flames generally have a stochastic character so that relatively long observation times are needed to quantify electric field effects. For example, lifted flames in electric fields can exhibit an oscillatory behavior where they alternately approach and recede from the burner exit until they finally reattach. Tens of seconds for this process is not unusual. Extended microgravity conditions will clarify the role of electric fields (via ion winds) on stability limits of flames.

3. EXPERIMENT REQUIREMENTS

3.1 Requirements Discussion

This section does not include any requirements, but instead describes their importance in achieving the experiment objectives. The requirements have been incorporated into the ACME-SRD-001 Integrated Science Requirements.

3.1.1 Ambient Environment

The experiments are to be conducted in the chamber described in the combined ACME science requirements. The gas fill for the gas jet tests and the coflow gas for the coflow burner tests is nominally nitrogen (79%) and oxygen (21%) by volume. For the coflow burner tests, the fill gas is as specified in the CLD Flame experiment SRD (as is the composition of the co-flow gas). Oxygen composition should not fall below 19% during the tests. Oxygen makeup gas can be added as it is consumed to maintain an appropriate overall oxygen concentration. The makeup oxygen is based on the assumption of complete combustion of the fuel flowing into the system. Because there is no direct oxygen concentration measurement, we expect that the chamber will be flushed and refilled approximately every 7-8 tests based on how much uncertainty has developed regarding the ambient oxygen concentration. We want to ensure that the oxygen level does not leave the window between 19 and 21%.

3.1.2 Burner Material

The gas-jet and coflow burners shall be electrically conductive and able to withstand a constant temperature of 1000 ºC. The burner temperature requirements reflect the maximum temperature observed at the burner tips in past laboratory 1-g experiments. The burner material requirement stems from the necessity of the burners to serve as electrodes in the high voltage circuit. Figure 2.4 illustrates how the burners complete the electrical pathway for measuring the flame's ion current by forcing electric current into a shunt resistor for measurement. The magnitude of the current is simply determined with Ohm's law and dividing the voltage drop across the resistor by the known value of the resistor.

3.1.3 Burners

Two different burner types are to be used. One is the simple gas jet burner. The second type is the coflow burner as specified in the CLD Flame experiment SRD. Two different nozzle diameters are included (one required and one desired) for the gas-jet burner to vary the exit velocity of the fuel mixture without altering the flow rates specified in each experimental test series and to match prior 1-g studies. The precise dimensions of all burner nozzles must be known to ensure accurate velocity computations and conditions for later numerical simulations by others if desired.

3.1.4 Electric Field

The electric field shall be produced between a copper mesh electrode and the burner. Copper mesh is an ideal electrode because its open surface area allows combustion gases to flow through preventing interaction with the flame. The range of mesh screen densities in the ACME science requirements have been used successfully in past experiments.

Another desired capability is to place the mesh electrode at a range of axial positions to achieve a desirable charge distribution in the electric field while preventing contact between the flame and the mesh. If the flame and mesh come into contact while the electric field is active, a short circuit will result, and the flame will allow electric current to flow between the burner and mesh electrode. Because the flame height and lift-off heights will vary across the two burners and the vast experimental conditions, variable positioning is highly desirable. A preliminary estimate of coflow burner lift-off heights suggests that the mesh be placed approximately 5 cm away from the burner nozzle, preferably at two different heights no less than 1 cm apart. The mesh diameter should be no less than 8 cm to collect sufficient ion current from the flame based on our electrokinetic calculations of ion flow. The electric field potential should be controllable in 50V or smaller increments and should be able to reach 10kV across the electrode space for both polarities.

3.1.5 Ion Current Measurement

The proposed method of ion current measurement involves measuring the voltage across a shunt resistor connected between the burner and the high voltage ground. Based on our past experiments, the resistor and data acquisition system should have a resolution better than 0.05 microamperes with an expected maximum current of 25 microamperes. For example, we suggest that the shunt resistor value shall be 100 kΩ, and will measure currents on the order of microamperes. The resulting voltage will be on the order of 0.1 Volt with an expected range of ± 4 Volts to be read by a 12-bit A/D converter. The resistor tolerance should better than or equal to ± 0.1%, and have the lowest possible temperature coefficient for precise measurements. The resistor should also be placed sufficiently far from the burners to prevent changes in the resistance value due to heat conduction through the connecting wire.

To ensure that the total ion current is measured at the shunt resistor, it is required that the mesh electrode and burner be electrically isolated to prevent current leakage. Current leakage should be less than 25 nanoamps at maximum voltage. The mesh electrode should withstand +/- 20kV without breaking down. In addition, it is suggested that a copper ring with a cross-sectional diameter of 2-3 mm be soldered to the perimeter of the mesh to reduce the likelihood of break down at the tips of the mesh wires at high voltages.

3.1.6 Flame Imaging and Chemiluminescence Measurements

Color images of the flame will reveal the flame area, provide evidence of combustion intensity, identify locations of soot formation, and show how the ion wind (local convection) changes the flame shape for the various input flame parameters and electric field strength. UV images with a filter for OH* are required to provide a sharp determination of the reaction zone. Images of CH* chemiluminescence are desired for observing spatial changes in heat release rate due to electric field actuation, and may also be used as a sensor for quantifying the electric field control effect. Density imaging is highly desired as this provides a secondary indication of the reaction zone location but more importantly shows the path of the convected hot gases driven by the ion wind for comparison with our electrokinetic modeling. It is also possible to extract temperature from density images in the soot-free regions of the flame, which is valuable for ascertaining electrical mobility. Density images should be at no less than 15 Hz.

3.1.7 Soot Measurements

Soot volume fraction and soot temperature are needed to show the effects of electric fields on the location, mean size, and amount of soot in the flames. Soot temperature provides information regarding the thermal field in highly sooting regions of the flame. The mean size of the soot is to be determined from assessing the presumed thermionic current from the soot. The ion current is related to soot surface area and so the mean size can be determined from the ratio of soot volume to soot area.

3.2 Operational Sequence

As described in Section 2, the E-FIELD experiment consists of 4 objectives corresponding to 4 series of tests using 2 different diffusion flame burner configurations. The first three test series provide the key fundamental information regarding the electrical character of diffusion flames and the influence of electric fields on soot formation; the final series focuses on electric field sensing and control of flames.

General Operations -- preparatory actions -- before any of the electric field experiments, the high voltage mesh should be installed (or moved into position). Leak current should be measured by sweeping the voltage from 0 to 10kV and 0 to -10kV with no flame present. A steep rise in current under these conditions indicates corona discharge and sets the upper limit on the potential. The test sequence involves a complete repeat voltage sweep with no flame to provide a point-by-point current leak measurement. A similar sweep should be completed following flame extinguishment at the end of a test set. The leak current allows a baseline for higher precision in the flame ion current determination. In addition, excessive leak current at relatively low voltage may indicate electron emission from carbon buildup on the gas jet flame tip. If the leak current exceeds 10% of the flame ion current, cleaning of the gas jet tip is requested. Cleaning consists of a manual wiping or possibly burning off the carbon with a modified flame condition. We expect this to be a rare request, but the continuous monitor of flameless ion current provides a reliable in-situ monitor. We assume that the chamber will be emptied and refilled approximately every 7-8 tests to minimize the oxygen concentration uncertainty in the test chamber. We further assume that our test series will start with the co-flow burner if it is already installed to minimize replacement time. After the co-flow experiments, a gas jet burner would be installed. The gas jet flame experiments duplicate our laboratory-based studies. The exact times for settling and voltage steps may vary (they should be reconfigurable from the ground), but a nominal expected operational sequence for one chamber fill and the key measurement data sets are shown below.

(A) Voltage Sweep – collection of *VI curves (or VCC curves)* -- where the voltage is swept from 0-±4kV (or until flame blowout) and the ion current is monitored and recorded. The sweep should be a series of discrete steps, where a settling time is allowed after each voltage change. At the same time, color and OH* video records the flame shape and luminosity (both broadband flame and soot luminosity and OH* chemiluminescence) throughout the sweep. Discrete steps in the sweep allow a system settling time and higher voltage resolution at some parts of the curve to effectively map the current transition points. A typical step sweep might comprise: 15 second ignition & stabilization; 100 V/step, 0.5 sec settle between steps, and a 0.3 sec. ion current measurement at each point, to ±5kV or blowout. It is important to keep in mind that the short measuring time is only possible because the changes are developing from a prior quasi-steady condition. If tests were attempted with a pair of voltage steps from a zero voltage initial condition (as in a drop test, for example), the settling time would more than double. Blowout can be detected by a sharp drop in ion current. Expected run times are 60 seconds per sweep (not including a background current sweep with the flame off). An example of this

kind of data was shown in Figures 1.10 and 2.2 for the ion current and Figures 1.5, 1.13, and 2.1 for the images.

Table 3.2.1

Voltage Sweep Procedure	**Time**
A. Prepare Chamber	
1. Fill chamber (with N_2 for coflow; O_2/N_2 for gas jet)	
2. Select fuel/diluent mixture	
B. Initiate Experiment	0 sec.
1. Initiate data acquisition	5 sec.
2. Initiate gas flows	5 sec
3. Ignite flame and retract igniter	8 sec.
4. Allow 10 seconds settling time	18 sec.
5. Set the desired voltage (initially to 0V)	19 sec.
6. Initiate high voltage power supply	20 sec.
C. Measurements	
1. Wait 0.3 seconds for flame to settle	
2. Collect data over 0.5 seconds	
D. Step 100V (assuming approx. 5ms ramp)	
E. Repeat steps C & D until (+/-) 5kV or flame blowout	60.25 sec.
F. Pause in Experiment	
1. Stop gas flows/extinguish flame (zero ion current)	
2. Stop video	
3. Zero voltage	
G. Repeat Steps C-E without flame to measure leakage current.	100.5 sec.
Stop testing if burner current leakage is at unacceptable level	
H. Reverse high voltage polarity	
I. Repeat sequence steps (B)–(H)	201 sec.

(B) ***Step Response***—where the voltage is changed rapidly from a base level to a much higher (or lower) level and the ion current (and flame luminosity and shape) is monitored in time as it settles to its new steady value. The key measurable is the ion current as a function of time through the voltage step change and the flame's subsequent settling. As in test set (A), video, luminosity, and chemiluminescence will record these flame behaviors in response to an instantaneous change in the electric field. A typical experiment sequence might comprise a 15 second ignition and stabilization, step changes on the order of hundreds of volts, and recording ion current for 2 seconds between step changes (where steps will not be limited to a single polarity). Settling time for these step changes in zero gravity (particularly, for soot related phenomena) may need to be adjusted via uplink; the test procedures shown are based on a nominal settling time observed in preliminary testing at 1-g and in the NASA Glenn 2.2 Second Drop Tower. The range of times between voltage steps may vary between 0-100 seconds. The two test series described above are carried out for a broad range of burner conditions (using up to 2 gas jet nozzles and the co-flow burner; fuel type variations between CH_4 and C_2H_4; and nitrogen dilution level of the fuel), and they provide the foundation necessary to create an electro-

dynamic model of the flame. The control input signals are flame luminosity (luminosity and CH* chemiluminescence) and ion current. Correlations between these two signals will also be examined. Once the dynamics of the flame has been determined from the VCC curves and the step response data; conditions will be selected for the examination and control of soot luminosity using electric fields will be performed. Finally, we will use electric fields to sense flame character and to control flame liftoff height and extend blowout limits in the co-flow burner.

Table 3.2.2

Step Response Procedure	**Time**
A. Prepare Chamber	
1. Fill chamber (with N_2 for coflow; O_2/N_2 for gas jet)	
2. Select fuel/diluent mixture	
B. Initate Experiment	
1. Initiate data acquisition	5 sec.
2. Start gas flows	5 sec.
3. Ignite flame and retract igniter	8 sec.
4. Allow 10 seconds settling time	18 sec.
5. Set the desired voltage (initially to 0V)	19 sec.
6. Initiate high voltage power supply	20 sec.
C. Measurements (if blowout occurs anytime; zero voltage and proceed to Step D)	
1. Collect data over 2 seconds	22 sec.
2. Step voltage 0V to 1000V; Collect data over 2 seconds	24 sec.
3. Step voltage 1000V to -1000V; Collect data over 2 seconds	26 sec.
4. Step voltage -1000V to 1000V; Collect data over 2 seconds	28 sec.
5. Step voltage 1000V to -2000V; Collect data over 2 seconds	30 sec.
6. Step voltage -2000V to 2000V; Collect data over 2 seconds	32 sec.
7. Step voltage 2000V to -2000V; Collect data over 2 seconds	34 sec.
8. Step voltage -2000V to 3000V; Collect data over 2 seconds	36 sec.
9. Step voltage 3000V to -3000V; Collect data over 2 seconds	38 sec.
10. Step voltage -3000V to 4000V; Collect data over 2 seconds	40 sec.
11. Step voltage 4000V to 5000V; Collect data over 2 seconds	42 sec.
12. Step voltage 5000V to 0V; Collect data over 2 seconds	44 sec.
13. Step voltage 0V to -4000V; Collect data over 2 seconds	46 sec.
14. Step voltage -4000V to -5000V; Collect data over 2 seconds	48 sec.
15. Step voltage -5000V to 0V; Collect data over 2 seconds	50 sec.
16. Step voltage 0V to -1000V; Collect data over 2 seconds	52 sec.
17. Step voltage -1000V to 0V; Collect data over 2 seconds	54 sec.
18. Step voltage 0V to -500V; Collect data over 2 seconds	56 sec.
19. Step voltage -500V to 0V; Collect data over 2 seconds	58 sec.
20. Step voltage 0V to 1000V; Collect data over 2 seconds	60 sec.
21. Step voltage 1000V to 500V; Collect data over 2 seconds	62 sec.
22. Step voltage 500V to 0V; Collect data over 2 seconds	64 sec.
D. Shut off gas flows (extinguish flame)	64 sec.
E. Repeat Step C beginning from 0V without flame to measure	106 sec.

leakage current. Stop testing and report if leakage is at unacceptable level	

(C) ***Electric Field Effects on Soot*** – demonstrate effects of the electric field on soot (measured by broadband emission from the flame and soot volume fraction) by slowly increasing the coflow air velocity while comparing the flame structure at each step to a flame affected purely by electric forcing. Conditions will be derived from experiments (A) and (B) above (time details: depends on the burner, but each test will be allowed at least 1 minute). Both broad solid angle collection luminosity and flame images will be used to determine the sooting behavior, along with soot volume fraction and soot pyrometry measurements for quantitative analysis.

Table 3.2.3

Electric Field Effects on Soot.	Time
A. Prepare Chamber	
1. Fill chamber (with N_2 for coflow; O_2/N_2 for gas jet)	
2. Select fuel/diluent mixture	
B. Initiate Experiment	
1. Initiate data acquisition	5 sec.
2. Start gas flows	5 sec.
3. Ignite flame and retract igniter	8 sec.
4. Allow 10 seconds settling time	18 sec.
C. Collect reference data for 1 second	21 sec.
D. Measurements	
1. Increase coflow velocity to 1cm/s; collect over 3 sec.	24 sec.
2. Increase coflow velocity to 2cm/s; collect over 3 sec.	27 sec.
3. Increase coflow velocity to 3cm/s; collect over 3 sec.	30 sec.
4. Increase coflow velocity to 4cm/s; collect over 3 sec.	33 sec.
5. Increase coflow velocity to 5cm/s; collect over 3 sec.	36 sec.
6. Increase coflow velocity to 6cm/s; collect over 3 sec.	39 sec.
7. Increase coflow velocity to 7cm/s; collect over 3 sec.	42 sec.
8. Increase coflow velocity to 8cm/s; collect over 3 sec.	45 sec.
9. Increase coflow velocity to 9cm/s; collect over 3 sec.	48 sec.
10. Increase coflow velocity to 10cm/s; collect over 3 sec.	51 sec.
11. Increase coflow velocity to 11cm/s; collect over 3 sec.	54 sec.
12. Increase coflow velocity to 12cm/s; collect over 3 sec.	57 sec.
13. Increase coflow velocity to 13cm/s; collect over 3 sec.	60 sec.
14. Increase coflow velocity to 14cm/s; collect over 3 sec.	63 sec.
15. Increase coflow velocity to 15cm/s; collect over 3 sec.	66 sec.
16. Increase coflow velocity to 16cm/s; collect over 3 sec.	69 sec.
17. Increase coflow velocity to 17cm/s; collect over 3 sec.	72 sec.
18. Increase coflow velocity to 18cm/s; collect over 3 sec.	75 sec.
19. Increase coflow velocity to 19cm/s; collect over 3 sec.	78 sec.
20. Increase coflow velocity to 20cm/s; collect over 3 sec.	81 sec.
21. Increase coflow velocity to 21cm/s; collect over 3 sec.	84 sec.

22. Increase coflow velocity to 22cm/s; collect over 3 sec.	87 sec.
23. Increase coflow velocity to 23cm/s; collect over 3 sec.	90 sec.
24. Increase coflow velocity to 24cm/s; collect over 3 sec.	93 sec.
25. Increase coflow velocity to 25cm/s; collect over 3 sec.	96 sec.
F. Stop gas flows/extinguish flame	

Note: return to step B and reignite as needed if flame fails during experiment

(D) ***Open Loop Sensing and Control*** – The experiments associated with control will be defined based on the results of the above baseline mapping experiments (A) and (B) above (time details: depends on the condition, but each test will be allowed at least 1 minute). After completing and evaluating the results, there are two sets of sensing and control experiments to be accomplished. The first is an open loop attempt to determine the strength of jet diffusion flames and the second is to extend the blowout limits of the co-flow flame and the second is to control formation. We will use the findings of the first two test series and the CLD Flame experiment to identify the conditions of flame sensitivity. The procedure is a series of voltage ramps (or small steps with continuous data collection); just to be sure there is no confusion at the end of the sequence, each step is identified but hopefully the pattern is clear. Ion current and luminosity (broadband and CH*) fluctuations will be used to determine the flame's approach to blowoff, and flame images will be used to determine the liftoff height. Note that fuel dilution with an inert may be necessary to allow flames to reach appropriate blowout conditions within experiment limitations.

Table 3.2.4

Open Loop Sensing and Control	Time
A. Prepare Chamber	
1. Fill chamber (with N_2 for coflow; O_2/N_2 for gas jet)	
2. Select fuel/diluent mixture	
B. Initiate Experiment	
1. Initiate data acquisition	5 sec.
2. Start gas flows	5 sec.
3. Ignite flame and retract igniter	8 sec.
4. Allow 10 seconds settling time	18 sec.
5. Set the desired voltage (initially to 0V)	19 sec.
6. Initiate high voltage power supply	20 sec.
C. Collect reference data for 1 second	21 sec.
D. Set voltage to V*, the initial (lifted or sooting) condition identified in prior tests	
E. Measurements	
1. Collect data over 1 seconds	22 sec.
2. Step voltage -300V to V*-300V; Collect data over 1.0 second	23 sec.
3. Ramp at +100V/s (or step +50V) while collecting data over 0.5 sec	23.5 sec.
4. Collect data at V*-250V over 1.0 second	24.5 sec.
5. Ramp at +100V/s (or step +50V) while collecting data over 0.5 sec	25 sec.
6. Collect data at V*-200V over 1.0 second	26 sec.
7. Ramp at +100V/s (or step +50V) while collecting data over 0.5 sec	26.5 sec.

8. Collect data at V*-150V over 1.0 second	27.5 sec.
9. Ramp at +100V/s (or step +50V) while collecting data over 0.5 sec	28 sec.
10. Collect data at V*-100V over 1.0 second	29 sec.
11. Ramp at +100V/s (or step +50V) while collecting data over 0.5 sec	29.5 sec.
12. Collect data at V*-50V over 1.0 second	30.5 sec.
13. Ramp at +100V/s (or step +50V) while collecting data over 0.5 sec	31 sec.
14. Collect data at V* over 1.0 second	32 sec.
15. Ramp at +100V/s (or step +50V) while collecting data over 0.5 sec	32.5 sec.
16. Collect data at V*+50V over 1.0 second	33.5 sec.
17. Ramp at +100V/s (or step +50V) while collecting data over 0.5 sec	34 sec.
18. Collect data at V*+100V over 1.0 second	35 sec.
19. Ramp at +100V/s (or step +50V) while collecting data over 0.5 sec	35.5 sec.
20. Collect data at V*+150V over 1.0 second	36.5 sec.
21. Ramp at +100V/s (or step +50V) while collecting data over 0.5 sec	37 sec.
22. Collect data at V*+200V over 1.0 second	38 sec.
23. Ramp at +100V/s (or step +50V) while collecting data over 0.5 sec	38.5 sec.
24. Collect data at V*+250V over 1.0 second	39.5 sec.
25. Ramp at +100V/s (or step +50V) while collecting data over 0.5 sec	40 sec.
26. Collect data at V*+300V over 1.0 second	41 sec.
27. Step to 0; collect data for 2 seconds	43 sec.
F. Stop gas flows/extinguish flame	43 sec.
G. Repeat Steps C-E with no flame to determine current leakage	65 sec.

* - Voltage level determined to affect soot or liftoff from previous experiments
Note: return to step B and reignite as needed if flame fails during experiment

The sequence would then repeat Steps B-H for following cases with given fuel/diluent mixture and change mixture as required. For the gas jet burner, open loop exploration will be allowed five minutes of total run time, and four conditions will be examined for soot control. For the co-flow burner, open loop exploration will be allowed 10 minutes of total run time, and eight conditions will be examined, four for soot control and four for liftoff/blowout.

3.3 Test Matrix

The two burners to be used are: (a) a simple gas jet nozzle with 2 sizes, 1.3 mm (required) and 2.1 mm diameter (required), and (b) a co-flow burner (same as in the CLD Flame study). The former jet nozzle size matches our ground-based configuration and the latter size matches the inner fuel tube of the co-flow burner. Some of the conditions in the co-flow burner test matrix intentionally match those proposed in the CLD Flame experiment to allow for future coordination and comparison. In all of the studies, the limiting commodity is oxygen for the system because the fuel use is very low in virtually all cases. There are four basic experimental activities involving electric field effects (VI curves, voltage step changes, soot response, and stability behavior response). The conditions for the latter two depend on the findings in the former two, and so the test matrix is

not definitive for these. Below is a table briefly summarizing the tests and the purpose of each. More details in this regard are in Section 2 under the description of the science data end products. Nominal and itemized test conditions planned for the co-flow burner and gas jet flames are in the table at the end of this document (E-FIELD Flames SRD). Specific test conditions may be altered, based on additional 1-g experiments.

Test type	Test Purpose
Voltage Sweep: 1.35 mm gas jet; 2.13 mm gas jet; co-flow burner; two fuels; 3 dilution conditions; 3 flow rates.	Identify flame shape changes, ion current per unit flame area, saturation current for fuel and dilution conditions, relationship between luminosity and electric field strength
Step Response: 1.35 mm gas jet; 2.13 mm gas jet; co-flow burner; two fuels; 3 dilution conditions; 3 flow rates.	Determine time response of the flame to sudden changes in electric field; provides the dynamic model for the flame to be used in control loops.
Electric field effects on soot: One gas jet and co-flow burner; 2 fuels; 3 dilution conditions	Determine response of soot to electric fields; distinguish ion wind effects from direct chemi-ion influences; evaluate soot contribution to ion current; demonstrate the ability of electric fields to control soot.
Open Loop Sensing and Control: co-flow burner; 2 fuels; 2 dilution conditions	Identify sensitive regions with the operating map where the electric field can change liftoff and stability behavior.

3.4 Success Criteria

Minimum Success:

- Obtain V-I curve in quasi-steady conditions for undiluted methane fuel on either diameter of the gas jet burner or the co-flow burner
- Simultaneously capture color images of flame responding to electric field during V-I sweep

Complete Success:

All of the above plus:

- Obtain V-I curve in quasi-steady conditions for both fuels (methane and ethylene) on one gas jet burner and the co-flow burner with a range of inert dilution of fuel
- Simultaneously capture flame images during voltage sweeps to allow measurement of liftoff height has a function of applied voltage
- Measure soot luminosity (radiometer measurement) as a function of applied voltage during VI sweeps and step changes
- Capture color images and soot luminosity (radiometer measurement) as a function of coflow velocity during Electric Field Effects on Soot experiment.

Superior Success:

All of the above plus:

- Demonstrate open loop control of flame near sooting and stability limits using ion current and luminosity as sensors by determining the decrease (or increase) in soot luminosity and by evaluating the extent to which stability limits can be extended using an electric field
- (Desired) Obtain thermal field information for the gas jet or coflow flame to visualize ion driven wind

3.5 Post-Flight Data Analysis

The post-flight data analysis will use many of the tools and follow many of the procedures established in our 1-g experiments, as shown in Section 1. In particular, we will employ electrokinetic modeling based on measured flame shapes and total ion currents, along with established relationships between flame area and ion flux to evaluate the links between flame behavior and chemi-ionization. Analysis of test results will be conducted both concurrently and at the conclusion of the flight experiment. Concurrent analysis is required at key points in the E-FIELD Flames test matrix to determine the specific test conditions and parameters necessary for a following set of related tests. Specifically, an analysis of ion current saturation, luminosity, and blowout will be conducted at the conclusion of the voltage sweep test sets (described in Section 3.2) to determine the best flow rate and nominal voltage range for soot effect tests and open-loop control tests. An analysis of step response experiments is also required to determine time constants for modeling the flame and designing the control parameters for open-loop experiments. Finally, an analysis of the near-limit test results in the E-FIELD Flames test matrix (and, desirably, the results of CLD Flame near-limit experiments) is required to determine the flow rate and mixtures that are most suitable for the stability experiments. It is important to note that while tentative conditions for soot effects and control tests have already been identified in the test matrix, the ability to select conditions based on analysis of previous tests will enhance the probability of success, and will ultimately maximize the value of the science product.

The final analysis of all experimental data will be conducted at the conclusion of the flight experiment until each objective (listed in Section 2.1) is achieved. Video, imagery (luminosity), thermal field information, and ion current data will be analyzed together to evaluate the ion wind strength, ion flux, ion production rate per unit carbon, and effects of electric fields on soot—completing Objectives A and C. Ion concentration will be determined from the saturation ion current: the point where ion collection and production are equal. The mobility can be determined from numerical methods previously discussed in Section 1 (see, for example, Figure 1.9) and in reference [52]. Once mobility is determined, we can ascertain the convective effects on the flame due to electricity.

One feature of the co-flow burner which makes this test unique is that axial convection on the flame is dominated by the forced flow (buoyant convection is removed). Hence, by reducing exit flow velocity and adjusting the magnitude of the electric potential at the mesh, it is possible to create an equivalent local flow velocity with different electrical effects. Adjustable flow configurations such as these would enable us to determine whether the electrical effects on soot are residence time based or chemical in nature.

Open loop control measurements allow us to understand the dominant factor in flame reattachment and extended blowout limits: is it the mean ion wind or mixing effects at the base? Analysis of the variation in ion current and luminosity time response in the step voltage experiments will be conducted to distinguish chemical effects of the electric field

from diffusion and ion wind since their timescales are sufficiently well separated. This analysis will fulfill Objective B. Objective D will be achieved by analyzing the effectiveness of the electric field to vary soot luminosity, vary lift-off heights, and delay extinction of a near-limit flame. All analyses completed during and after the flight experiment will be documented in anticipation for future disclosure.

4. REFERENCES

1. A.M. Starik and N.S. Titova. Kinetics of ion formation in the volumetric reaction of methane with air. *Combustion, Explosion, and Shock Waves*, 38(3):253–268, 2002.

2. Pedersen, T. and Brown, R.C. (1993) "Simulation of electric field effects in premixed methane flames. *Combust. Flame*, **94**, 433–448.

3. J.A. Green, T.M. Sugden, Some observations on the mechanism of ionization in flames containing hydrocarbons, in: Ninth Symposium (International) on Combustion, Academic Press, New York, 1963, pp. 607±621.

4. Peeters, J., Vinkier, C., and Van Tiggelen, A., Formation and Behaviour of Chemi-Ions in Flames, *Oxidat. Combust. Rev.,* vol. 4, 93-132 (1969).

5. F.L. Jones, P.M. Becker, R.J. Heinsohn, A mathematical model of the opposed-jet diffusion flame: effect of an electric field on concentration and temperature profiles, Combust. Flame 19, (1972) 351-362.

6. J. Prager, U. Riedel, J. Warnatz, "Modeling ion chemistry and charged species diffusion in lean methane–oxygen flames," *Proceedings of the Combustion Institute* 31 (2007) 1129–1137.

7. Lawton J. and Weinberg F.J. 1969. Electrical Aspects of Combustion. Clarendon Press. Oxford.

8. Dunn-Rankin, D. and Weinberg, F.J. "Using Large Electric Fields to Control Transport in Microgravity," Annals of the New York Academy of Sciences, Vol. 1077, 570—584, 2006.

9. Papac, M.J. and Dunn-Rankin, D. "Canceling Buoyancy of Gaseous Fuel Flames in a Gravitational Environment Using an Ion-Driven Wind," Annals of the New York Academy of Sciences, Vol. 1077, 585—601, 2006.

10. Lawton, J. and Weinberg F.J. 1964. Maximum ion currents from flames and the maximum practical effects of applied electric fields. *Proc. Roy. Soc. London. A*, 2**77**(1371): 468-497.

11. Sher, E., Pinhasi, G., Pokryvailo, A., and Bar-on, R., 1993, "Extinction of Pool Flames by Means of a DC Electric Field," *Combust. Flame*, **94**, 244–252.

12. Carleton, F.B. and Weinberg, F.J., "Electric Field-Induced Flame Convection in the Absence of Gravity," *Nature*, **330**, 635 (1987).

13. Hu, J., Riven, B. and Sher, E. (2000) "The effect of an electric field on the shape of co-flowing and candle-type methane-air flames," *Exp. Therm Fluid Sci.*, **21**, 124–133.

14. Mayo, P.J., and Weinberg, F.J. “On the Size, Charge and Number-Rate of Formation of Carbon Particles in Flames Subjected to Electric Fields,” *Proceedings of the Royal Society of London. Series A, Mathematical and Physical Sciences*, Vol. 319, No. 1538, 351—371, 1970.

15. Kono, M., Carleton, F.B., Jones, A.R., and Weinberg, F.J. “The effect of nonsteady electric-fields on sooting flames.” *Combustion and Flame*, 78:357--364, 1989.

16. Saito, M., Sato, M., and Sawada, K. Variation of flame shape and soot emission by applying electric field. *Journal of Electrostatics*, 39:305–311, 1997.

17. H.C. Jaggers, A. von Engel, The effect of electric fields on the burning velocity of various flames, *Combust. Flame* 16 (1971) 275-285.

18. H.C. Jaggers, R.J. Boeser, F.J. Weinberg, The effect of electric fields on burning velocity, *Combust. Flame* 19 (1972), 135-136.

19. Sher, E., Pokryvailo, A., Jacobson, E., and Mond, M. “Extinction of Flames in a Nonuniform Electric-Field,” *Combustion Science and Technology*, vol. 87 (1-6): 59—67, 1993.

20. Calcote, H.F. and Pease, R.N. “Electrical Properties of Flames – Burner Flames in Longitudinal Electric Fields,” Industrial and Engineering Chemistry, vol. 43 (12): 2726—2731, 1951.

21. Panteleev, A.F., Popkov, G.A., Shebko, Y.N., and Tsarichenko, S.G., “Effect of AC Field on the Limiting Blow-Off Flow-Rate Value for a Diffusion Propane Hydrogen Flame,” Combustion Explosion and Shock Waves, vol. 29 (1): 32—33, 1993.

22. Yuan ZG, Hegde U, Faeth GM “Effects of electric fields on non-buoyant spherical diffusion flames,” Combustion and Flame 124 (4): 712-716, 2001.

23. H.F. Calcote and D.G. Keil. The role of ions in soot formation. *Pure Appl. Chem.*, 62(5):815–824, 1990.

24. Boothman, D., Lawton, J., Melinek, S.J., and Weinberg, F.J. 1969. Rates of ion generation in flames. *In* 12th Symposium (International) on Combustion. 969-977. The Combustion Institute.

25. Mehresh P, Souder J, Flowers D, Riedel, U., and Dibble, R.W. “Combustion timing in HCCI engines determined by ion-sensor: experimental and kinetic modeling,” Proceedings of the Combustion Institute 30: 2701-2709 Part 2 2005.

26. Weinberg, F.J., “Electrically Driven Convection,” *Proc. 1st International Symposium on Fluids in Space,* (Ajaccio, November, 1991), ESA SP-353, 123 (1992).

27. Carleton, F.B. and Weinberg, F.J., "Simulation of microgravity by the application of electric fields to flames," *Joint meeting of the Portuguese, British, Spanish, and Swedish Sections of The Combustion Institute, Madeira*, 8.5.1 (1996)

28. Strayer B.A , Posner, J.D., Dunn-Rankin D., and Weinberg F.J., "Simulating microgravity in small diffusion flames by using electric fields to counterbalance natural convection"

29. Strayer, B.A. and Dunn-Rankin, D. (2001) "Response of a Non-Premixed Flame to Electric Field Forcing," 18th International Colloquium on the Dynamics of Explosions and Reactive Systems, Seattle, Washington, July 29--August 3.

30. Borgatelli, F. and Dunn-Rankin, D. (2006) "Feedback Control of Ion Current from a Small Diffusion Flame," Paper 06S-44, Western States Section/The Combustion Institute Spring Meeting, University of Idaho, Boise, March 27--28.

31. Sandhu, S.S. and Weinberg, F.J "Laser Interferometric Studies of the Control of Heat Transfer from Flame Gases by Electric Fields," Combustion and Flame, Vol. 25, 321—334, 1975.

32. Strayer, B.A. and Dunn-Rankin, D. "Control of the Vaporization Rate in a Droplet Stream Flame using Electric Fields," *Proceedings of NHTC'01, the 35th ASME National Heat Transfer Conference*, Anaheim, California, June (2001).

33. Papac, M.J., Dunn-Rankin, D., Stipe, C.B., and Lucas, D. "N2 CARS thermometry and O2 LIF concentration measurements in a flame under electrically induced microbuoyancy," Combustion and Flame, Vol. 133, 241—254, 2003.

34. Papac, M.J. "Effects of Electric Fields on Convection in Combustion Plasmas and Surrounding Gases," Paper AIAA-2005-4784 of the 36th *AIAA Plasmadynamics and Lasers Conference*, Toronto, June (2005).

35. Yamashita, K, Karnani, S., and Dunn-Rankin, D. (2009) "Numerical Prediction of Ion Current from a Small Methane Jet Flame," Combustion and Flame, 156: 1227-1233.

36. Karnani, S. and Dunn-Rankin, D.. Electric field effects on a small co-flow diffusion flame. In Proceedings of the 6th U.S. National Combustion Meeting, Ann Arbor, MI, May 17-20, 2009 2009.

37. Takahashi, F. and Katta, V.. Structure of propagating edge diffusion flames in hydrocarbon fuel jets. Proceedings of the Combustion Institute, 30:375–382, 2005.

38. Karnani, S., Schoen, M., Coffin, P., Dunn-Rankin, D., Takahashi, F., Yuan, Z.-G., and Stocker, D.. Exploring the effects of gravity on a coflow diffusion flame in an electric field. Fall Technical Meeting of the Western States Section of the Combustion Institute at University of California, Irvine, Oct 26-27 2009.

39. Bennett, M., Borgatelli, F. and Dunn-Rankin, D. (2007) "Behavior of Non-Premixed Flames as Electrically Active Components in a High-Voltage Circuit," 21st International Colloquium on Dynamics of Explosions and Reactive Systems, Poitiers, France, July 23--27.

40. Place, E.R. and Weinberg, F.J. "Electrical Control of Flame Carbon," *Proceedings of the Royal Society of London. Series A, Mathematical and Physical Sciences,* Vol. 289, No. 1417, 192—205, 1966.

41. Saito, M., Arai, T., and Arai, M. Control of soot emitted from acetylene diffusion flames by applying an electric field. *Combustion and Flame*, 119:356–366, 1999.

42. Unterreiner, B.V., Sierka, M., and Ahlrichs, R. (2004) "Reaction pathways for growth of polycyclic aromatic hydrocarbons under combustion conditions, a DFT study," *Phys. Chem. Chem. Phys.*, **6**, 4377—4384.

43. P. Pandey, B.P. Pundir, P.K. Panigrahi (2007) "Hydrogen addition to acetylene–air laminar diffusion flames: Studies on soot formation under different flow arrangements," *Combustion and Flame*, **148**, 249—262.

44. Weilmunster, P., Keller, A., Homann, K.-H. (1999) "Large Molecules, Radicals, Ions, and Small Soot Particles in Fuel-Rich Hydrocarbon Flames, Part I: Positive Ions of Polycyclic Aromatic Hydrocarbons (PAH) in Low-Pressure Premixed Flames of Acetylene and Oxygen, *Combustion and Flame*, 116: 62—83.

45. Leszczynski, J., Wiseman, F., and Zerner, M.C. (1988) "Toward an Ionic Mechanism of Soot Particle Formation: Reactions Between Acetylene and Tautomeric Forms of the C3H3+ Ions, *International Journal of Quantum Chemistry: Quantum Chemistry Symposium,* **22***,* 117—125.

46. Won, S.H., Cha, M.S., Park, C.S., and Chung, S.H. "Effect of electric fields on reattachment and propagation speed of tribrachial flames in laminar coflow jets," Proceedings of the Combustion Institute, 31, 963—970, 2007.

47. Won, S.H., Ryu, S.K., Cha, M.S., Kim, J.S., and Chung, S.H. "Propagation of Tribrachial Flames in Electric Fields," 21st ICDERS Conference, Poitiers, France, July 23—27, 2007.

48. Cheng, T.S., Cheng, C.P., Chen, C.S., Li, Y.H., Wu, C.Y., and Chao, Y.C. "Characteristics of microjet methane diffusion flames," Combustion Theory and Modelling, Vol. 10, No. 5, 861—881, 2006.

49. Smooke, M.D., Long, M.B., Connelly, B.C., Colket, M.B., and Hall, R.J. "Soot formation in laminar diffusion flames," Combustion and Flame, Vol. 143, 613—628, 2005.

50. Smooke, M.D., Hall, R.J., Colket, M.B., Fielding, J., Long, M.B., McEnally, C.S., and Pfefferle, L.D., "Investigation of the transition from lightly sooting towards heavily

sooting co-flow ethylene diffusion flames," Combustion Theory and Modelling, Vol. 8, 593—606, 2004.

51. Walsh, K.T., Fielding, J., Smooke, M.D., Long, M.B., and Linan, A. "A comparison of computational and experimental lift-off heights of coflow laminar diffusion flames," Proceedings of the Combustion Institute, Vol. 30, 357—365, 2005.

52. Papac, M.J. and Dunn-Rankin, D. "Modelling Electric Field Driven Convection in Small Combustion Plasmas and Surrounding Gases," Combustion Theory and Modelling, in press, 2007.

53. Payne, K.G. and Weinberg, F.J. "A Preliminary Investigation of Field-Induced Ion Movement in Flame Gases and Its Applications," *Proceedings of the Royal Society of London. Series A, Mathematical and Physical Sciences*, Vol. 250, No. 1262, 316—336, 1959.

54. Ryu, S.K., Kim, Y.K., and Chung, S.H. "Effect of Electric Fields on Reattachment of Lifted Flame at Low AC Frequency," Paper A38, 5th US Combustion Meeting, San Diego, CA, March 25—28, 2007.

55. Yuan, Z.G. and Hegde, U. "Recent Advances in Electric Field Effects on Diffusion Flames in a Spherically Symmetric System," AIAA Aerospace Sciences Meeting Paper AIAA-2003-0812, 2003.

56. Sunderland, P.B., Axelbaum, R.L., Urban, D.L., Chao, B.H., and Liu, S. Effects of structure and hydrodynamics on the sooting behavior of spherical microgravity diffusion flames. *Combustion and Flame*, 132:25–33, 2003.

57. Bahadori, M.Y., Stocker, D.P., Zhou, L., and Hegde, U. (2001) "Radiative loss from non-premixed flames in reduced-gravity environments," Combustion Science and Technology, 167: 169-186.